

# On the Block-Diagonalization and Multiplicative Equivalence of Quaternion Z-Block Circulant Matrices with their Applications

Daochang Zhang<sup>a</sup>, Yue Zhao<sup>b</sup>, Jingqian Li<sup>c</sup>, Dijana Mosić<sup>d</sup>

<sup>a</sup> College of Sciences, Northeast Electric Power University, Jilin 132012, P.R. China.

E-mail: [daochangzhang@126.com](mailto:daochangzhang@126.com)

<sup>b</sup> Department of Math & Stat, Georgia State University, Atlanta, GA 30303, USA.

E-mail: [yuezhao0303@163.com](mailto:yuezhao0303@163.com)

<sup>c</sup> College of Sciences, Northeast Electric Power University, Jilin 132012, P.R. China.

E-mail: [JingqianLi85@163.com](mailto:JingqianLi85@163.com)

<sup>d</sup> Faculty of Sciences and Mathematics, University of Niš, P.O. Box 224, 18000 Niš, Serbia.

E-mail: [dijana@pmf.ni.ac.rs](mailto:dijana@pmf.ni.ac.rs)

---

## Abstract

The motivation of this paper is twofold. First, we investigate the block-diagonalization of the  $z$ -block circulant matrix  $\mathbf{bcirc}_z(\mathcal{A})$ , based on this block-diagonal structure, and develop the algorithm  $\mathbf{bcirc}_z\text{-inv}$  for computing the inverse of  $\mathbf{bcirc}_z(\mathcal{A})$ . Second, we establish the equivalence between the QT-product of tensors and the product of the corresponding  $z$ -block circulant matrices. Based on this equivalence and in combination with the algorithm  $\mathbf{bcirc}_z\text{-inv}$ , large-scale tests and scalability analysis of the Tikhonov-regularized model are conducted.

As a by-product of the analysis, some relevant and straightforward properties of the quaternion  $z$ -block circulant matrices are provided. As applications, a series of quaternion tensor decompositions under the QT-product and their corresponding  $z$ -block circulant matrices decompositions are obtained, including the QT-Polar decomposition, the QT-PLU decomposition, and the QT-LU decomposition. Meanwhile, the QT-SVD is rederived based on the relation between  $\mathcal{A}$  and  $\mathbf{bcirc}_z(\mathcal{A})$ . Furthermore, we develop corresponding algorithms and present several large-scale tests and scalability analysis. In addition, applications in video rotation are presented to evaluate several rotation strategies based on the QT-Polar decomposition, which shows the decomposition remains stable and inter-frame consistent while accurately maintaining color reproduction.

**Keywords:** Z-Block Circulant Matrices, Block-Diagonalization, Multiplicative Equivalence, Quaternion Tensors, QT-Product, Decompositions

**2010 MSC:** 15A69; 15A72; 65F30; 94A08; 97N30

---

## 1. Introduction

Quaternion algebra, introduced by Hamilton in 1843 to address the problem of representing rotations in a three-dimensional space within mechanics, generalizes the complex numbers to four dimensions. It forms an associative yet noncommutative algebra. The fundamental multiplication relations,  $\mathbf{ij} = \mathbf{k}$ ,  $\mathbf{jk} = \mathbf{i}$ , and  $\mathbf{ki} = \mathbf{j}$ , naturally encode the algebraic structure of the cross product in  $\mathbb{R}^3$ . Moreover, quaternions constitute a skew field, preserving the essential algebraic properties that underlie linear and spectral analysis, Fourier transforms, and other foundational constructions in signal processing and applied mathematics.

The expressive power of quaternion algebra has led to extensive applications in signal and image processing [20], robotics [4], computer graphics [24], and texture analysis [14]. In particular, a quaternion matrix provides an efficient representation of color images, where the three imaginary components correspond to the RGB channels. This compact representation facilitates algebraic operations on color data, motivating the development of quaternion-based matrix and tensor decompositions.

Tensors provide a natural generalization of matrices to higher-order arrays and offer a powerful framework for modeling multidimensional data in signal processing, color image processing, facial recognition, and computer vision [11, 19, 26, 30, 20, 17]. The theoretical foundations of tensor decomposition were comprehensively reviewed by Kolda and Bader [13]. With the introduction of new tensor products such as the Einstein product [5], the T-product [12], and the QT-product [22], tensor decompositions defined under these products have attracted increasing research interest.

It is worth noting that most existing studies on tensor decompositions based on various products are formulated over the complex field. Classical tensor decomposition models, including the CANDECOMP/PARAFAC (CP) decomposition [2], the Tucker decomposition [27], the higher-order singular value decomposition (HOSVD) [15], and the tensor singular value decomposition (t-SVD) [12] have been extensively investigated. Recently, there have been several new generalizations about the SVD in the quaternion division ring, including the quaternion tensor singular value decomposition (QT-SVD) [22], the tensor generalized singular value decomposition (T-QGSVD) [9] and the constrained quaternion singular value decomposition [3]. On the other hand, the QT-QR decomposition was introduced in [18, 23]. Moreover, the polar decomposition of tensors with the Einstein product was investigated in [6].

Particularly, [12] showed that the normalized Discrete Fourier Transform (DFT) matrix block-diagonalizes any complex block circulant matrix. And the multiplicative equivalence between the product of the block circulant matrices of tensors and the T-product of their associated quaternion tensors holds.

Two key observations can be made.

- (i) The above multiplicative equivalence breaks down under the QT-product. How can we find the equivalence between the product of certain matrices of tensors and the QT-product of the corresponding tensors?
- (ii) If such a matrix of a tensor is found, which can keep the multiplicative equivalence under the QT-product. Can it also be block-diagonalized? Since both [21] and [34] demonstrated that the quaternion block circulant matrix can be block-diagonalized.

Therefore, this paper aims to introduce the known cross structure of the circulant matrix associated with the quaternion tensor  $\mathcal{A}$ , which, for convenience, is referred to as the  $z$ -block circulant matrix of  $\mathcal{A}$ , denoted by  $\mathbf{bcirc}_z(\mathcal{A})$ , and explore its block-diagonalization. Furthermore, this directly leads to the computational equivalence between the product of the  $z$ -block circulant matrices and the QT-product of their corresponding quaternion tensors. The specific content is organized as follows.

In Section 2, we review the relevant definitions and present several key lemmas on third-order quaternion tensors, which form the theoretical foundation for the subsequent sections.

In Section 3, we establish the block-diagonalization of the  $z$ -block circulant matrix of  $\mathcal{A}$  denoted by  $\mathbf{bcirc}_z(\mathcal{A})$ , and to establish the equivalence between the QT-product of tensors and the product of their corresponding  $z$ -block circulant matrices. The essential properties of quaternion  $z$ -block circulant matrices are then analyzed.

In Section 4, we first propose the QT-Polar decomposition, the QT-PLU decomposition, the QT-LU decomposition, and their corresponding  $z$ -block circulant matrices decompositions via the properties as mentioned in Section 3. Then we present several numerical examples to verify the accuracy. In addition, we rederive the QT-SVD by using the relation between  $\mathcal{A}$  and  $\mathbf{bcirc}_z(\mathcal{A})$ , which removes an additional unnecessary restriction appearing in the proof of [22, Theorem 2.2], where assumed that  $\text{diag}(\hat{\mathcal{S}})$  is diagonal.

Section 5 first presents a  $z$ -block circulant structure-accelerated inversion algorithm ( $\mathbf{bcirc}_z\text{-inv}$ ) for computing the inverse of  $\mathbf{bcirc}_z(\cdot)$ , followed by a set of large-scale tests and scalability analysis, some of which compare the proposed algorithms with several alternative methods.

In Section 6, large-scale experiments and scalability analysis of the Tikhonov-regularized model are conducted using Theorem 3.4 and the algorithm  $\mathbf{bcirc}_z\text{-inv}$ . Subsequently, a practical example is presented to illustrate video rotation via quaternion tensor polar decomposition, which demonstrates that the QT-polar decomposition preserves frame-to-frame coherence while maintaining stability and faithful color reproduction.

## 2. Preliminaries and key lemmas

In this section, we present a concise summary of the key definitions and notations used in the subsequent analysis.

For clarity and consistency, throughout this paper, we first introduce the notations that [22] adopted.

We adopt the conventions that scalars by lowercase letters  $a, b, \dots$ , vectors by bold lowercase letters  $\mathbf{a}, \mathbf{b}, \dots$ , matrices by uppercase letters  $A, B, \dots$ , and third-order tensors by calligraphic letters  $\mathcal{A}, \mathcal{B}, \dots$ . In addition,  $A^*$  and  $\mathcal{A}^*$  represent the conjugate transpose of the matrix  $A$  and the third-order tensor  $\mathcal{A}$ , separately. For a third-order tensor  $\mathcal{A}$ , we employ MATLAB-style indexing that is  $i$ -th horizontal slice  $\mathcal{A}(i, :, :)$ ,  $j$ -th lateral slice  $\mathcal{A}(:, j, :)$ , and  $k$ -th frontal slice  $\mathcal{A}(:, :, k)$ . For concise, we denote the  $k$ -th frontal slice by  $\mathcal{A}^{(k)} := \mathcal{A}(:, :, k)$ .

Let  $\mathbb{R}$  denote the field of real numbers, and  $\mathbb{C}$  the field of complex numbers. The set  $\mathbb{Q}$  of quaternions forms a four-dimensional vector space on  $\mathbb{R}$ , with the ordered basis  $\mathbf{1}, \mathbf{i}, \mathbf{j}, \mathbf{k}$ .

A quaternion  $q \in \mathbb{Q}$  can be written in the form

$$q = q_0 + q_1\mathbf{i} + q_2\mathbf{j} + q_3\mathbf{k},$$

where  $q_0, q_1, q_2, q_3 \in \mathbb{R}$ , and the imaginary units  $\mathbf{i}, \mathbf{j}, \mathbf{k}$  satisfy the following multiplication rules:

$$\begin{cases} \mathbf{i}^2 = \mathbf{j}^2 = \mathbf{k}^2 = -1, \\ \mathbf{ij} = -\mathbf{ji} = \mathbf{k}, \\ \mathbf{jk} = -\mathbf{kj} = \mathbf{i}, \\ \mathbf{ki} = -\mathbf{ik} = \mathbf{j}. \end{cases}$$

Moreover, the conjugate of a quaternion  $q$  is defined as  $q^* = q_0 - q_1\mathbf{i} - q_2\mathbf{j} - q_3\mathbf{k}$ , and its norm is given by  $|q| = \sqrt{q^*q} = \sqrt{q_0^2 + q_1^2 + q_2^2 + q_3^2}$ . Note that any quaternion  $q$  can be regarded as a two-dimensional vector over complex field  $\mathbb{C}$ , and can be uniquely expressed as

$$q = c_1 + jc_2,$$

where  $c_1 = q_0 + q_1\mathbf{i}$  and  $c_2 = q_2 - q_3\mathbf{i}$ .

Let  $\mathbb{Q}^n$  denote the set of  $n$ -dimensional quaternion vectors. Similarly, let  $Q \in \mathbb{Q}^{m \times n}$  represent the set of  $m \times n$  quaternion matrices. Any quaternion matrix can be expressed in the form

$$Q = Q_{\mathbf{d}} + \mathbf{j}Q_{\mathbf{c}},$$

where  $Q_{\mathbf{d}}, Q_{\mathbf{c}} \in \mathbb{C}^{m \times n}$ .

Next, we present the definition of eigenvalues for quaternion matrices, following the discussion in [32].

**Definition 2.1.** *Given a quaternion matrix  $A \in \mathbb{Q}^{n \times n}$ , if there exists a nonzero quaternion vector  $x \in \mathbb{Q}^n$  and a scalar  $\lambda \in \mathbb{Q}$  such that*

$$Ax = x\lambda \quad (\text{respectively, } Ax = \lambda x),$$

*then  $\lambda$  is called a right (respectively, left) eigenvalue of  $A$ , and  $x$  is the corresponding right (left) eigenvector.*

Since quaternion multiplication is non-commutative, eigenvalues of quaternion matrices are classified as left and right eigenvalues, which generally have no direct relationship. In this work, we consider only right eigenvalues.

Furthermore, let  $\mathcal{A} \in \mathbb{Q}^{n_1 \times n_2 \times n_3}$  be a third-order quaternion tensor, represented as

$$\mathcal{A} = \mathcal{A}_{\mathbf{d}} + \mathbf{j}\mathcal{A}_{\mathbf{c}}, \quad (1)$$

where  $\mathcal{A}_{\mathbf{d}}, \mathcal{A}_{\mathbf{c}} \in \mathbb{C}^{n_1 \times n_2 \times n_3}$ . We define **bcirc** as the block circulant matrix associated with  $\mathcal{A}$ , of size  $n_1 n_3 \times n_2 n_3$ , given by:

$$\text{bcirc}(\mathcal{A}) := \begin{bmatrix} \mathcal{A}^{(1)} & \mathcal{A}^{(n_3)} & \mathcal{A}^{(n_3-1)} & \dots & \mathcal{A}^{(2)} \\ \mathcal{A}^{(2)} & \mathcal{A}^{(1)} & \mathcal{A}^{(n_3)} & \dots & \mathcal{A}^{(3)} \\ \vdots & \vdots & \vdots & \ddots & \vdots \\ \mathcal{A}^{(n_3)} & \mathcal{A}^{(n_3-1)} & \mathcal{A}^{(n_3-2)} & \dots & \mathcal{A}^{(1)} \end{bmatrix}$$

Moreover, the operation **unfold** maps a tensor  $\mathcal{A} \in \mathbb{Q}^{n_1 \times n_2 \times n_3}$  into an  $n_1 n_3 \times n_2$  block column vector, corresponding to the first block column of **bcirc**( $\mathcal{A}$ ). The inverse operation, denoted **fold**, reconstructs the original tensor from its unfolded representation. These operations are defined as follows [12]:

$$\text{unfold}(\mathcal{A}) := \begin{bmatrix} \mathcal{A}^{(1)} \\ \mathcal{A}^{(2)} \\ \vdots \\ \mathcal{A}^{(n_3)} \end{bmatrix}, \quad \text{fold}(\text{unfold}(\mathcal{A})) := \mathcal{A}.$$

It is well-known that the normalized Discrete Fourier Transform (DFT) matrix diagonalizes any complex circulant matrix [8]. Consequently, for any tensor  $\mathcal{A} \in \mathbb{C}^{n_1 \times n_2 \times n_3}$ , we have

$$(F_{n_3} \otimes I_{n_1}) \text{bcirc}(\mathcal{A}) (F_{n_3}^* \otimes I_{n_2}) = \begin{bmatrix} \hat{\mathcal{A}}^{(1)} & & & \\ & \hat{\mathcal{A}}^{(2)} & & \\ & & \ddots & \\ & & & \hat{\mathcal{A}}^{(n_3)} \end{bmatrix} := \text{diag}(\hat{\mathcal{A}}), \quad (2)$$

where  $\hat{\mathcal{A}}^{(s)}$ ,  $s = 1, 2, \dots, n_3$  are frontal slices of  $\hat{\mathcal{A}}$ .  $F_{n_3} \in \mathbb{C}^{n_3 \times n_3}$  is the normalized DFT matrix, where  $F_{n_3}(i, j) = n_3^{-1/2} \omega^{(i-1)(j-1)}$  such that  $i, j \in 1, 2, \dots, n_3$  and  $\omega = e^{\frac{-2\pi i}{n_3}}$ . Additionally, for any quaternion tensor  $\mathcal{A} \in \mathbb{Q}^{n_1 \times n_2 \times n_3}$ , applying the DFT to  $\mathcal{A}$  results in a quaternion tensor  $\hat{\mathcal{A}} \in \mathbb{Q}^{n_1 \times n_2 \times n_3}$ , where

$$\begin{aligned}\hat{\mathcal{A}}(i, j, :) &= \sqrt{n_3} F_{n_3} \mathcal{A}(i, j, :) = \sqrt{n_3} F_{n_3} \mathcal{A}_{\mathbf{d}}(i, j, :) + \mathbf{j} \sqrt{n_3} P_{n_3} F_{n_3} \mathcal{A}_{\mathbf{c}}(i, j, :) \\ &= \hat{\mathcal{A}}_{\mathbf{d}}(i, j, :) + \mathbf{j} P_{n_3} \hat{\mathcal{A}}_{\mathbf{c}}(i, j, :)\end{aligned}\quad (3)$$

such that  $i \in 1, 2, \dots, n_1$  and  $j \in 1, 2, \dots, n_2$ . In addition, the permutation matrix  $P_{n_3} = (P_{ij}) \in \mathbb{R}^{n_3 \times n_3}$  is defined as  $P_{11} = 1$  and

$$P_{ij} = \begin{cases} 1, & \text{if } i + j = n_3 + 2, \quad 2 \leq i, j \leq n_3, \\ 0, & \text{otherwise.} \end{cases}$$

The above operation (3) is represented by a command  $fftq(\cdot)$ , i.e.,  $\hat{\mathcal{A}} = fftq(\mathcal{A}, [ ], 3)$ . Its inverse operation is  $\mathcal{A} = ifftq(\hat{\mathcal{A}}, [ ], 3)$ . Then we have the following routine computation:

$$\text{unfold}(\hat{\mathcal{A}}) = \sqrt{n_3} (F_{n_3} \otimes I_{n_1}) \text{unfold}(\mathcal{A}) \text{ and } \text{unfold}(\mathcal{A}) = \frac{1}{\sqrt{n_3}} (F_{n_3}^* \otimes I_{n_1}) \text{unfold}(\hat{\mathcal{A}}) \quad (4)$$

as also discussed in [22].

In what follows, we present several crucial definitions and lemmas. First, we present the definition of the QT-product as follows:

**Definition 2.2.** [22] Let  $\mathcal{A}_{\mathbf{d}}, \mathcal{A}_{\mathbf{c}} \in \mathbb{C}^{n_1 \times r \times n_3}$ , and consider tensors  $\mathcal{A} = \mathcal{A}_{\mathbf{d}} + \mathbf{j} \mathcal{A}_{\mathbf{c}} \in \mathbb{Q}^{n_1 \times r \times n_3}$  and  $\mathcal{B} \in \mathbb{Q}^{r \times n_2 \times n_3}$ . Here, the symbol  $\otimes$  denotes the Kronecker product. We define

$$\mathcal{A} *_Q \mathcal{B} \doteq \text{fold} \left( (\text{bcirc}(\mathcal{A}_{\mathbf{d}}) + \mathbf{j} \text{bcirc}(\mathcal{A}_{\mathbf{c}}) \cdot (P_{n_3} \otimes I_r)) \cdot \text{unfold}(\mathcal{B}) \right) \in \mathbb{Q}^{n_1 \times n_2 \times n_3}.$$

We present several basic definitions that will be used frequently in the following sections.

**Definition 2.3.** [22] The  $n \times n \times n_3$  identity quaternion tensor  $\mathcal{I}_{nnn_3}$  is the tensor whose first frontal slice is the identity matrix, and whose remaining frontal slices are zero matrices.

**Definition 2.4.** [22] The  $n \times n \times n_3$  quaternion tensor  $\mathcal{U}$  is said to be unitary if

$$\mathcal{U}^* *_Q \mathcal{U} = \mathcal{U} *_Q \mathcal{U}^* = \mathcal{I}_{nnn_3}.$$

**Definition 2.5.** [22] The tensor  $\mathcal{P} \in \mathbb{Q}^{n \times n \times n_3}$  is called an f-diagonal quaternion tensor if each of its frontal slices is a diagonal quaternion matrix.

**Definition 2.6.** [18] The tensor  $\mathcal{P} \in \mathbb{Q}^{n \times n \times n_3}$  is called an f-upper (lower)-triangular quaternion tensor if each of its frontal slices is an upper (lower)-triangular quaternion matrix.

Now, the conjugate transpose of a third-order tensor over the complex field is defined as follows.

**Definition 2.7.** [12] Let  $\mathcal{A} \in \mathbb{C}^{n_1 \times n_2 \times n_3}$ . Its conjugate transpose  $\mathcal{A}^* \in \mathbb{C}^{n_2 \times n_1 \times n_3}$  is defined by conjugately transposing each frontal slice of  $\mathcal{A}$  and reversing the order of slices 2 through  $n_3$ .

Next, we introduce the notion of the conjugate transpose of a third-order quaternion tensor.

**Definition 2.8.** [22] The conjugate transpose of a quaternion tensor  $\mathcal{A} = \mathcal{A}_{\mathbf{d}} + \mathbf{j} \mathcal{A}_{\mathbf{c}} \in \mathbb{Q}^{n_1 \times n_2 \times n_3}$ , denoted by  $\mathcal{A}^* \in \mathbb{Q}^{n_2 \times n_1 \times n_3}$ , is defined by

$$\text{unfold}(\mathcal{A}^*) = \text{unfold}(\mathcal{A}_{\mathbf{d}}^*) - (P_{n_3} \otimes I_{n_2}) \text{unfold}(\mathcal{A}_{\mathbf{c}}^*) \mathbf{j}.$$

### 3. Block-Diagonalization and Multiplicative Equivalence of Quaternion $Z$ -Block Circulant Matrices

In this section, we first introduce the known cross structure of the circulant matrix of the quaternion tensor  $\mathcal{A}$ , for convenience, called the  $z$ -block circulant matrix and denoted by  $\text{bcirc}_z(\mathcal{A})$ , and then investigate its block-diagonalization.

**Definition 3.1 (Z-Block Circulant Matrix).** Let  $\mathcal{A} \in \mathbb{Q}^{n_1 \times r \times n_3}$ ,  $\mathcal{A}_d \in \mathbb{C}^{n_1 \times r \times n_3}$ , and  $\mathcal{A}_c \in \mathbb{C}^{n_1 \times r \times n_3}$  satisfy that

$$\mathcal{A} = \mathcal{A}_d + \mathbf{j}\mathcal{A}_c \in \mathbb{Q}^{n_1 \times r \times n_3}.$$

Then the  $z$ -block circulant matrix of  $\mathcal{A}$  is defined by  $\text{bcirc}_z(\mathcal{A})$  as follows:

$$\text{bcirc}_z(\mathcal{A}) = \text{bcirc}(\mathcal{A}_d) + \mathbf{j}\text{bcirc}(\mathcal{A}_c)(P_{n_3} \otimes I_r), \quad (5)$$

where  $P_{n_3}$  is as defined in Definition 2.2.

Based on Definition 3.1, we conclude that the explicit structure of the  $z$ -block circulant matrix  $\text{bcirc}_z(\mathcal{A})$  is as follows:

$$\text{bcirc}_z(\mathcal{A}) = \begin{bmatrix} \mathcal{A}_d^{(1)} + \mathbf{j}\mathcal{A}_c^{(1)} & \mathcal{A}_d^{(n_3)} + \mathbf{j}\mathcal{A}_c^{(2)} & \cdots & \mathcal{A}_d^{(2)} + \mathbf{j}\mathcal{A}_c^{(n_3)} \\ \mathcal{A}_d^{(2)} + \mathbf{j}\mathcal{A}_c^{(2)} & \mathcal{A}_d^{(1)} + \mathbf{j}\mathcal{A}_c^{(3)} & \cdots & \mathcal{A}_d^{(3)} + \mathbf{j}\mathcal{A}_c^{(1)} \\ \mathcal{A}_d^{(3)} + \mathbf{j}\mathcal{A}_c^{(3)} & \mathcal{A}_d^{(2)} + \mathbf{j}\mathcal{A}_c^{(4)} & \cdots & \mathcal{A}_d^{(4)} + \mathbf{j}\mathcal{A}_c^{(2)} \\ \vdots & \vdots & \ddots & \vdots \\ \mathcal{A}_d^{(n_3)} + \mathbf{j}\mathcal{A}_c^{(n_3)} & \mathcal{A}_d^{(n_3-1)} + \mathbf{j}\mathcal{A}_c^{(1)} & \cdots & \mathcal{A}_d^{(1)} + \mathbf{j}\mathcal{A}_c^{(n_3-1)} \end{bmatrix}. \quad (6)$$

In what follows, we provide a concise and transparent relation between  $\text{bcirc}_z(\mathcal{A})$  and  $\text{diag}(\hat{\mathcal{A}})$  in the quaternion division ring as follows.

**Theorem 3.2.** Let  $\mathcal{A}_d$  and  $\mathcal{A}_c \in \mathbb{C}^{n_1 \times n_2 \times n_3}$  satisfy that  $\mathcal{A} = \mathcal{A}_d + \mathbf{j}\mathcal{A}_c \in \mathbb{Q}^{n_1 \times n_2 \times n_3}$ . Denote that  $\hat{\mathcal{A}}$  is the DFT of  $\mathcal{A}$ . Then,

$$(F_{n_3} \otimes I_{n_1})\text{bcirc}_z(\mathcal{A})(F_{n_3}^* \otimes I_{n_2}) = \text{diag}(\hat{\mathcal{A}}). \quad (7)$$

*Proof.* Recall that the DFT matrix  $F_{n_3}$  satisfies  $F_{n_3}F_{n_3}^* = P_{n_3}$ , where  $P_{n_3}$  is a permutation matrix. Moreover, the conjugate of  $F_{n_3}$ , denoted  $\bar{F}_{n_3}$ , satisfies  $\bar{F}_{n_3} = F_{n_3}^*$ . Then, we conclude that

$$F_{n_3}\mathbf{j} = \mathbf{j}\bar{F}_{n_3} = \mathbf{j}F_{n_3}^* = \mathbf{j}F_{n_3}^*(F_{n_3}F_{n_3}^*) = \mathbf{j}P_{n_3}F_{n_3}.$$

In addition, the following equations are helpful for computation:

$$F_{n_3}P_{n_3} = P_{n_3}F_{n_3} = F_{n_3}^*, \quad F_{n_3}^*P_{n_3} = P_{n_3}F_{n_3}^* = F_{n_3}.$$

Substituting (5) into the left-hand side of (7), we obtain

$$\begin{aligned} & (F_{n_3} \otimes I_{n_1})(\text{bcirc}_z(\mathcal{A}))(F_{n_3}^* \otimes I_{n_2}) \\ &= (F_{n_3} \otimes I_{n_1})(\text{bcirc}(\mathcal{A}_d) + \mathbf{j}\text{bcirc}(\mathcal{A}_c)(P_{n_3} \otimes I_{n_2}))(F_{n_3}^* \otimes I_{n_2}) \\ &= (F_{n_3} \otimes I_{n_1})\text{bcirc}(\mathcal{A}_d)(F_{n_3}^* \otimes I_{n_2}) + (F_{n_3} \otimes I_{n_1})\mathbf{j}\text{bcirc}(\mathcal{A}_c)(F_{n_3} \otimes I_{n_2}) \end{aligned} \quad (8)$$

It is worth noting that the matrix-form identity  $(UV) \otimes (YW) = (U \otimes Y)(V \otimes W)$ . Moreover, we observe that  $(F_{n_3} \otimes I_{n_1})\mathbf{j} = (F_{n_3}\mathbf{j} \otimes I_{n_1}) = (\mathbf{j}F_{n_3}^* \otimes I_{n_1}) = \mathbf{j}(F_{n_3}^* \otimes I_{n_1}) = \mathbf{j}(F_{n_3}P_{n_3} \otimes I_{n_1})$ , then (8) can be reformulate as

$$\begin{aligned} & (F_{n_3} \otimes I_{n_1})\left(\mathbf{bcirc}_z(\mathcal{A})\right)(F_{n_3}^* \otimes I_{n_2}) \\ &= (F_{n_3} \otimes I_{n_1})\mathbf{bcirc}(\mathcal{A}_d)(F_{n_3}^* \otimes I_{n_2}) + \mathbf{j}(F_{n_3} \otimes I_{n_1})(P_{n_3} \otimes I_{n_1})\mathbf{bcirc}(\mathcal{A}_c)(F_{n_3}^* \otimes I_{n_2})(P_{n_3} \otimes I_{n_2}). \end{aligned}$$

Therefore, combining (2) and (3), the above equation can be rewritten as

$$(F_{n_3} \otimes I_{n_1})\left(\mathbf{bcirc}_z(\mathcal{A})\right)(F_{n_3}^* \otimes I_{n_2}) = \text{diag}(\hat{\mathcal{A}}_d) + \mathbf{j}(P_{n_3} \otimes I_{n_1})\text{diag}(\hat{\mathcal{A}}_c)(P_{n_3} \otimes I_{n_2}) = \text{diag}(\hat{\mathcal{A}}).$$

Hence, the proof is completed.  $\square$

We now proceed to define the following two inverse operations.

The operator  $\text{diag}^{-1}(\cdot)$  denotes the inverse of  $\text{diag}(\cdot)$ :

$$\text{diag}^{-1}\left(\begin{bmatrix} \hat{\mathcal{A}}_{(1)} & & & \\ & \hat{\mathcal{A}}_{(2)} & & \\ & & \ddots & \\ & & & \hat{\mathcal{A}}_{(n_3)} \end{bmatrix}\right) = \hat{\mathcal{A}}.$$

The operator  $\mathbf{bcirc}_z^{-1}(\cdot)$  is defined as the inverse of  $\mathbf{bcirc}_z(\cdot)$ :

$$\mathcal{A} = \mathbf{bcirc}_z^{-1}\left(\begin{bmatrix} \mathcal{A}_d^{(1)} + \mathbf{j}\mathcal{A}_c^{(1)} & \mathcal{A}_d^{(n_3)} + \mathbf{j}\mathcal{A}_c^{(2)} & \dots & \mathcal{A}_d^{(2)} + \mathbf{j}\mathcal{A}_c^{(n_3)} \\ \mathcal{A}_d^{(2)} + \mathbf{j}\mathcal{A}_c^{(2)} & \mathcal{A}_d^{(1)} + \mathbf{j}\mathcal{A}_c^{(3)} & \dots & \mathcal{A}_d^{(3)} + \mathbf{j}\mathcal{A}_c^{(1)} \\ \mathcal{A}_d^{(3)} + \mathbf{j}\mathcal{A}_c^{(3)} & \mathcal{A}_d^{(2)} + \mathbf{j}\mathcal{A}_c^{(4)} & \dots & \mathcal{A}_d^{(4)} + \mathbf{j}\mathcal{A}_c^{(2)} \\ \vdots & \vdots & \ddots & \vdots \\ \mathcal{A}_d^{(n_3)} + \mathbf{j}\mathcal{A}_c^{(n_3)} & \mathcal{A}_d^{(n_3-1)} + \mathbf{j}\mathcal{A}_c^{(1)} & \dots & \mathcal{A}_d^{(1)} + \mathbf{j}\mathcal{A}_c^{(n_3-1)} \end{bmatrix}\right).$$

**Remark 3.3.** Let  $\mathcal{A} = \mathcal{A}_d + \mathbf{j}\mathcal{A}_c \in \mathbb{Q}^{n_1 \times n_2 \times n_3}$ , where  $\mathcal{A}_d, \mathcal{A}_c \in \mathbb{C}^{n_1 \times n_2 \times n_3}$ . The tensor  $\hat{\mathcal{A}} \in \mathbb{Q}^{n_1 \times n_2 \times n_3}$  is obtained by applying the DFT to  $\mathcal{A}_d$  and  $\mathcal{A}_c$  along the third mode. Then

$$\text{fftq}(\mathcal{A}, [ ], 3) = \hat{\mathcal{A}} = \text{id} \text{diag}((F_{n_3} \otimes I_{n_1})\mathbf{bcirc}_z(\mathcal{A})(F_{n_3}^* \otimes I_{n_2})).$$

$$\text{ifftq}(\hat{\mathcal{A}}, [ ], 3) = \mathcal{A} = \text{ibcirc}_z((F_{n_3}^* \otimes I_{n_2})\text{diag}(\hat{\mathcal{A}})(F_{n_3} \otimes I_{n_1})).$$

Next, we establish the multiplicative equivalence between  $z$ -block circulant matrices and their corresponding quaternion tensors under the QT-product as follows.

**Theorem 3.4.** Let  $\mathcal{A} \in \mathbb{Q}^{n_1 \times r \times n_3}$ ,  $\mathcal{B} \in \mathbb{Q}^{r \times n_2 \times n_3}$ , and  $\mathcal{C} \in \mathbb{Q}^{n_1 \times n_2 \times n_3}$ . Then

$$\mathcal{A} *_Q \mathcal{B} = \mathcal{C} \iff \mathbf{bcirc}_z(\mathcal{A})\mathbf{bcirc}_z(\mathcal{B}) = \mathbf{bcirc}_z(\mathcal{C}).$$

*Proof.* From the definitions of QT-product and  $\mathbf{bcirc}_z$ , we have

$$\mathcal{A} *_Q \mathcal{B} = \text{fold}(\mathbf{bcirc}_z(\mathcal{A})\text{unfold}(\mathcal{B})).$$

Furthermore, taking `unfold` operation on both sides, we obtain

$$\begin{aligned}\text{unfold}(\mathcal{A} *_Q \mathcal{B}) &= \text{bcirc}_z(\mathcal{A})\text{unfold}(\mathcal{B}) \\ &= \frac{1}{\sqrt{n_3}}\text{bcirc}_z(\mathcal{A})(F_{n_3}^* \otimes I_r)\text{unfold}(\hat{\mathcal{B}}),\end{aligned}\quad (9)$$

and the second equality is derived from (4). In addition, we can still get the following equality by utilizing (4),

$$\begin{aligned}\widehat{\text{unfold}(\mathcal{A} *_Q \mathcal{B})} &= \sqrt{n_3}(F_{n_3} \otimes I_{n_1})\text{unfold}(\mathcal{A} *_Q \mathcal{B}) \\ &= (F_{n_3} \otimes I_{n_1})\text{bcirc}_z(\mathcal{A})(F_{n_3}^* \otimes I_r)\text{unfold}(\hat{\mathcal{B}}),\end{aligned}$$

where the second equality is obtained by substituting  $\text{unfold}(\mathcal{A} *_Q \mathcal{B})$  with (9). By utilizing Theorem 3.2, it directly follows that

$$\begin{aligned}(F_{n_3} \otimes I_{n_1})\text{bcirc}_z(\mathcal{A} *_Q \mathcal{B})(F_{n_3}^* \otimes I_{n_2}) \\ = (F_{n_3} \otimes I_{n_1})\text{bcirc}_z(\mathcal{A})(F_{n_3}^* \otimes I_r)(F_{n_3} \otimes I_r)\text{bcirc}_z(\mathcal{B})(F_{n_3}^* \otimes I_{n_2}),\end{aligned}$$

which implies

$$\text{bcirc}_z(\mathcal{A} *_Q \mathcal{B}) = \text{bcirc}_z(\mathcal{A})\text{bcirc}_z(\mathcal{B}).$$

Hence, the proof is complete.  $\square$

**Remark 3.5.** It is worth mentioning that [22] discussed the following relationship when  $\mathcal{A} \in \mathbb{Q}^{n_1 \times r \times n_3}$ ,  $\mathcal{B} \in \mathbb{Q}^{r \times n_2 \times n_3}$ , and  $\mathcal{C} \in \mathbb{Q}^{n_1 \times n_2 \times n_3}$  under the QT-product:

$$\mathcal{A} *_Q \mathcal{B} = \mathcal{C} \iff \text{diag}(\hat{\mathcal{A}})\text{diag}(\hat{\mathcal{B}}) = \text{diag}(\hat{\mathcal{C}}),$$

where  $\hat{\mathcal{A}}$ ,  $\hat{\mathcal{B}}$ , and  $\hat{\mathcal{C}}$  are the DFT of  $\mathcal{A}$ ,  $\mathcal{B}$ , and  $\mathcal{C}$ , respectively.

Based on Theorem 3.2, it follows immediately that

$$\begin{array}{ccc}\text{bcirc}_z(\mathcal{C}) = \text{bcirc}_z(\mathcal{A})\text{bcirc}_z(\mathcal{B}) & \longleftrightarrow & \text{diag}(\hat{\mathcal{C}}) = \text{diag}(\hat{\mathcal{A}})\text{diag}(\hat{\mathcal{B}}) \\ \longleftrightarrow & & \longleftrightarrow \\ \mathcal{C} = \mathcal{A} *_Q \mathcal{B} & & \end{array}$$

However, we can not obtain the above conclusion without Theorem 3.2.

In addition, we discuss the conjugate transpose equivalence between the quaternion tensor  $\mathcal{A}$  and the  $z$ -block circulant matrix  $\text{bcirc}_z(\mathcal{A})$ .

**Theorem 3.6.** Let  $\mathcal{A} \in \mathbb{Q}^{n \times n \times n_3}$  and the conjugate transpose of  $\mathcal{A}$  is defined by  $\mathcal{A}^*$ . Then

$$\text{bcirc}_z(\mathcal{A}^*) = \text{bcirc}_z(\mathcal{A})^*.$$

*Proof.* Observe that the structure of  $\mathcal{A}^*$  is as follows:

$$\text{unfold}(\mathcal{A}^*) = \text{unfold}(\mathcal{A}_d^*) - (P_{n_3} \otimes I_n)\text{unfold}(\mathcal{A}_c^*)\mathbf{j}.$$

Then, by Definition 3.1, we provide the  $z$ -block circulant matrix of  $\mathcal{A}^*$

$$\mathbf{bcirc}_z(\mathcal{A}^*) = \mathbf{bcirc}(\mathcal{A}_d^*) + \mathbf{jbcirc}(-\mathcal{A}_c^T)(P_{n_3} \otimes I_n), \quad (10)$$

where  $\mathcal{A}_c^T$  is the transpose of  $\mathcal{A}_c$ . Moreover, we can rewrite (10) as follows:

$$\begin{aligned} \mathbf{bcirc}_z(\mathcal{A}^*) &= \mathbf{bcirc}(\mathcal{A}_d^*) - \mathbf{bcirc}(\mathbf{j}\mathcal{A}_c^T)(P_{n_3} \otimes I_n) \\ &= \mathbf{bcirc}(\mathcal{A}_d^*) - \mathbf{bcirc}\left(\mathbf{fold}\left((P_{n_3} \otimes I_n)\mathbf{unfold}(\mathcal{A}_c^*)\right)\mathbf{j}(P_{n_3} \otimes I_n)\right) \\ &= \mathbf{bcirc}(\mathcal{A}_d^*) - (P_{n_3} \otimes I_n)\mathbf{bcirc}(\mathcal{A}_c^*)\mathbf{j}, \end{aligned} \quad (11)$$

where the third equality is obtained from

$$\mathbf{bcirc}\left(\mathbf{fold}\left((P_{n_3} \otimes I_n)\mathbf{unfold}(\mathcal{A}_c^*)\right)\right) = (P_{n_3} \otimes I_n)\mathbf{bcirc}(\mathcal{A}_c^*)(P_{n_3} \otimes I_n).$$

Additionally, from Definition 3.1, we conclude that

$$\begin{aligned} \mathbf{bcirc}_z(\mathcal{A})^* &= \mathbf{bcirc}(\mathcal{A}_d)^* - (P_{n_3} \otimes I_n)\mathbf{bcirc}(\mathcal{A}_c)^*\mathbf{j} \\ &= \mathbf{bcirc}(\mathcal{A}_d^*) - (P_{n_3} \otimes I_n)\mathbf{bcirc}(\mathcal{A}_c^*)\mathbf{j}, \end{aligned} \quad (12)$$

and the second equality follows from the structure of the block circulant matrix, that is  $\mathbf{bcirc}(\mathcal{A}_d^*) = \mathbf{bcirc}(\mathcal{A}_d)^*$ . Therefore, it is directly verified that (11) coincides with (12), thereby completing the proof.  $\square$

**Remark 3.7.** We state the following identity:

$$\mathbf{bcirc}_z(\mathcal{A}^*) = \mathbf{bcirc}_z(\mathcal{A})^* \iff \mathbf{diag}(\widehat{\mathcal{A}}^*) = \mathbf{diag}(\widehat{\mathcal{A}})^*.$$

However,  $\mathbf{diag}(\widehat{\mathcal{A}}^*) \neq \mathbf{diag}(\widehat{\mathcal{A}})^*$ .

Then we discuss the unitary relation between the quaternion tensor  $\mathcal{A}$  and the  $z$ -block circulant matrix  $\mathbf{bcirc}_z(\mathcal{A})$ .

**Corollary 3.8.** A quaternion tensor  $\mathcal{A} \in \mathbb{Q}^{n \times n \times n_3}$  is unitary if and only if  $\mathbf{bcirc}_z(\mathcal{A})$  is unitary.

*Proof.* Suppose that  $\mathbf{bcirc}_z(\mathcal{A})$  is unitary. Then it follows that

$$\mathbf{bcirc}_z(\mathcal{A})\mathbf{bcirc}_z(\mathcal{A})^* = \mathbf{bcirc}_z(\mathcal{A})^*\mathbf{bcirc}_z(\mathcal{A}) = I_{nn_3}.$$

By utilizing Theorem 3.6 and Theorem 3.4, we obtain

$$\begin{aligned} \mathbf{bcirc}_z(\mathcal{A})\mathbf{bcirc}_z(\mathcal{A}^*) &= \mathbf{bcirc}_z(\mathcal{A}^*)\mathbf{bcirc}_z(\mathcal{A}) = I_{nn_3} \\ \iff \mathcal{A} *_Q \mathcal{A}^* &= \mathcal{A}^* *_Q \mathcal{A} = \mathcal{I}_{nnn_3}. \end{aligned}$$

Thus, the condition is necessary and sufficient.  $\square$

**Remark 3.9.** It is worth noting that, based on Corollary 3.8, it follows immediately that

$$\begin{aligned} \mathbf{bcirc}_z(\mathcal{A})\mathbf{bcirc}_z(\mathcal{A})^* &= \mathbf{bcirc}_z(\mathcal{A})^*\mathbf{bcirc}_z(\mathcal{A}) = I_{nn_3} \\ \iff \mathcal{A} *_Q \mathcal{A}^* &= \mathcal{A}^* *_Q \mathcal{A} = \mathcal{I}_{nnn_3} \\ \iff \text{diag}(\hat{\mathcal{A}})\text{diag}(\hat{\mathcal{A}})^* &= \text{diag}(\hat{\mathcal{A}})^*\text{diag}(\hat{\mathcal{A}}) = I_{nn_3}. \end{aligned}$$

where the second necessary and sufficient condition was investigated in [22] using a different approach. However, we can not obtain the above conclusion without Theorem 3.6.

It is well known that a quaternion tensor  $\mathcal{A} \in \mathbb{Q}^{n \times n \times n_3}$  is Hermitian if and only if  $\mathcal{A}^* = \mathcal{A}$ , or equivalently,  $\text{unfold}(\mathcal{A}) = \text{unfold}(\mathcal{A}^*)$ . Then we can provide the following theorem directly.

**Theorem 3.10.** Let  $\mathcal{H} \in \mathbb{Q}^{n \times n \times n_3}$  and let  $\mathbf{bcirc}_z(\mathcal{H})$  denote the  $z$ -block circulant matrix of  $\mathcal{H}$ . Then

$$\mathcal{H} \text{ is Hermitian} \iff \mathbf{bcirc}_z(\mathcal{H}) \text{ is Hermitian.}$$

*Proof.* We first show the sufficiency.

By Theorem 3.6, if  $\mathbf{bcirc}_z(\mathcal{H})$  is Hermitian, then

$$\mathbf{bcirc}_z(\mathcal{H}^*) = \mathbf{bcirc}_z(\mathcal{H})^* = \mathbf{bcirc}_z(\mathcal{H}).$$

It is obvious that  $\mathbf{bcirc}_z$  is an invertible map, i.e.,

$$\mathcal{H}^* = \mathbf{bcirc}_z^{-1}(\mathbf{bcirc}_z(\mathcal{H})^*) = \mathbf{bcirc}_z^{-1}(\mathbf{bcirc}_z(\mathcal{H})) = \mathcal{H}.$$

We now prove the necessity.

If  $\mathcal{H}$  is Hermitian, by Theorem 3.6, we obtain

$$\mathbf{bcirc}_z(\mathcal{H})^* = \mathbf{bcirc}_z(\mathcal{H}^*) = \mathbf{bcirc}_z(\mathcal{H}).$$

Combining the two directions, the statement follows.  $\square$

## 4. Quaternion tensor decompositions via QT-product

This section aims to generalize some classic decompositions of quaternion matrices to quaternion tensors based on the QT-product. We begin by introducing several definitions. Furthermore, we present the polar decomposition of quaternion tensors via the QT-product. To facilitate the subsequent discussion, we define f-positive definite (semidefinite) of Hermitian quaternion tensors based on [32, Corollary 6.1 and Corollary 6.2].

**Definition 4.1.** [32] An  $n \times n$  Hermitian matrix  $A$  is said to be positive (semidefinite) if  $x^*Ax > (\geq) 0$  for all nonzero column vectors  $x$  of  $n$  quaternion components.

By Definition 4.1, we present the following definition.

**Definition 4.2 (F-Positive Definite (Semidefinite)).** A Hermitian quaternion tensor  $\mathcal{A} \in \mathbb{Q}^{n \times n \times n_3}$  is called f-positive definite (semidefinite) if each frontal slice of  $\mathcal{A}$  is positive definite (semidefinite).

**Remark 4.3.** [32] Let  $A \in \mathbb{Q}^{n \times n}$  with standard eigenvalues  $h_1 + k_1\mathbf{i}, \dots, h_n + k_n\mathbf{i}$  such that the right spectrum  $\sigma_r(A) = [h_1 + k_1\mathbf{i}] \cup \dots \cup [h_n + k_n\mathbf{i}]$ .  $A$  is normal if and only if there exists a unitary matrix  $U$  such that

$$U^*AU = \text{diag}\{h_1 + k_1\mathbf{i}, h_2 + k_2\mathbf{i}, \dots, h_n + k_n\mathbf{i}\} = D,$$

and  $A$  is Hermitian if and only if  $k_i = 0$  for  $1 \leq i \leq n$ .

Moreover,  $A$  is Hermitian positive definite (semidefinite) if and only if  $h_i > 0$  ( $h_i \geq 0$ ) and  $k_i = 0$  for  $1 \leq i \leq n$ .

It is worth noting that the left polar decomposition for quaternion matrices was presented in [32, Theorem 7.1]. Utilizing the argument used in [32, Theorem 7.1], one can analogously show that there exist a unitary quaternion matrix  $U$  and a Hermitian positive semidefinite quaternion matrix  $H$  such that the right polar decomposition of a quaternion matrix  $A$  can be expressed as  $A = UH$ . In what follows, we present the next theorem.

**Theorem 4.4 (QT-(Right) Polar decomposition).** Let  $\mathcal{A} \in \mathbb{Q}^{n \times n \times n_3}$ . Then there exist a unitary quaternion tensor  $\mathcal{U}$ , and a Hermitian and f-positive semidefinite quaternion tensor  $\mathcal{H}$  such that

$$\mathcal{A} = \mathcal{U} *_Q \mathcal{H}.$$

In the meantime,

$$\text{bcirc}_{\mathbf{z}}(\mathcal{A}) = \text{bcirc}_{\mathbf{z}}(\mathcal{U})\text{bcirc}_{\mathbf{z}}(\mathcal{H}),$$

where  $\text{bcirc}_{\mathbf{z}}(\mathcal{U})$  is unitary, and  $\text{bcirc}_{\mathbf{z}}(\mathcal{H})$  is Hermitian and positive semidefinite.

*Proof.* From the right polar decomposition of a quaternion matrix, we obtain  $\hat{\mathcal{A}}^{(i)} = \hat{\mathcal{U}}^{(i)}\hat{\mathcal{H}}^{(i)}$ , where  $\hat{\mathcal{H}}^{(i)}$  is Hermitian and positive semidefinite, and  $\hat{\mathcal{U}}^{(i)}$  is unitary. Moreover, for each  $1 \leq i \leq n_3$  and every nonzero vector  $x^{(i)} \in \mathbb{Q}^n$ , we have

$$(x^{(i)})^*\hat{\mathcal{H}}^{(i)}x^{(i)} \geq 0.$$

Notice that  $\hat{\mathcal{A}}^{(i)}$ ,  $\hat{\mathcal{H}}^{(i)}$ , and  $\hat{\mathcal{U}}^{(i)}$  denote the  $i$ -th frontal slice of  $\hat{\mathcal{A}}$ ,  $\hat{\mathcal{H}}$ , and  $\hat{\mathcal{U}}$ , respectively. Then we have

$$\text{diag}(\hat{\mathcal{A}}) = \text{diag}(\hat{\mathcal{U}})\text{diag}(\hat{\mathcal{H}}), \quad (13)$$

where  $\text{diag}(\hat{\mathcal{U}})$  is unitary and  $\text{diag}(\hat{\mathcal{H}})$  is Hermitian with

$$x^*\text{diag}(\hat{\mathcal{H}})x \geq 0, \quad x = \begin{bmatrix} x^{(1)} \\ x^{(2)} \\ \vdots \\ x^{(n_3)} \end{bmatrix}, \quad (14)$$

which implies  $\text{diag}(\hat{\mathcal{H}})$  is positive semidefinite.

By Theorem 3.2, we have

$$\text{bcirc}_{\mathbf{z}}(\mathcal{U}) = (F_{n_3}^* \otimes I_n)\text{diag}(\hat{\mathcal{U}})(F_{n_3} \otimes I_n),$$

then  $\text{bcirc}_z(\mathcal{U})$  is unitary. Furthermore, by Corollary 3.8, we obtain  $\mathcal{U}$  is unitary.

By applying Theorem 3.2 and equation (13), we derive

$$\text{bcirc}_z(\mathcal{A}) = \text{bcirc}_z(\mathcal{U})\text{bcirc}_z(\mathcal{H}). \quad (15)$$

Furthermore, utilizing Theorem 3.2, we observe that

$$\text{bcirc}_z(\mathcal{H}) = (F_{n_3}^* \otimes I_n) \text{diag}(\hat{\mathcal{H}})(F_{n_3} \otimes I_n),$$

it follows that

$$\text{bcirc}_z(\mathcal{H})^* = (F_{n_3}^* \otimes I_n) \text{diag}(\hat{\mathcal{H}})^*(F_{n_3} \otimes I_n),$$

and since  $\text{diag}(\hat{\mathcal{H}})$  is Hermitian, we conclude that  $\text{bcirc}_z(\mathcal{H})$  is Hermitian. Then, by Theorem 3.4, Theorem 3.10 and equation (4), we obtain  $\mathcal{A} = \mathcal{U} *_Q \mathcal{H}$ , where  $\mathcal{H}$  is Hermitian and f-positive semidefinite.

On the other hand, by equation (14) and Theorem 3.2, we obtain

$$x^*(F_{n_3} \otimes I_n) \text{bcirc}_z(\mathcal{H})(F_{n_3}^* \otimes I_n)x \geq 0.$$

Let  $(F_{n_3}^* \otimes I_n)x = y$ , and thus  $y^* = x^*(F_{n_3} \otimes I_n)$ . Since  $x$  is arbitrary,  $y$  is arbitrary as well. Consequently,

$$y^* \text{bcirc}_z(\mathcal{H}) y \geq 0,$$

where  $\text{bcirc}_z(\mathcal{H})$  is Hermitian and positive semidefinite.  $\square$

Based on the preceding theorem, we next present an algorithm for computing the QT-Polar decomposition, stated in Algorithm 1.

---

#### Algorithm 1 QT-Polar

---

**Input:** Third-order quaternion tensor  $\mathcal{A} \in \mathbb{Q}^{n \times n \times n_3}$

**Output:** Third-order unitary tensor  $\mathcal{U} \in \mathbb{Q}^{n \times n \times n_3}$ , and Hermitian and f-positive semidefinite tensor  $\mathcal{H} \in \mathbb{Q}^{n \times n \times n_3}$ .

```

1:  $\hat{\mathcal{A}} = \text{fftq}(\mathcal{A}, [ ], 3)$ 
2: for  $i = 1, 2, \dots, n_3$  do  $[\hat{\mathcal{U}}(:, :, i), \hat{\mathcal{H}}(:, :, i)] = \text{Polar}(\hat{\mathcal{A}}(:, :, i))$ 
3: end for
4:  $\mathcal{U} = \text{ifftq}(\hat{\mathcal{U}}, [ ], 3)$ ,  $\mathcal{H} = \text{ifftq}(\hat{\mathcal{H}}, [ ], 3)$ 

```

---

To verify the accuracy of Algorithm 1 for computing the QT-Polar decomposition, we present the following example.

**Example 4.5.** Let  $\mathcal{A} = \mathcal{A}_d + j\mathcal{A}_c \in \mathbb{Q}^{3 \times 3 \times 2}$  with entries

$$\mathcal{A}_d(:, :, 1) = \begin{bmatrix} 8 & 3 + 8i & 6 + 6i \\ 2 & 2 + 10i & 5 + 5i \\ 10 + 5i & 2 + 1i & 3 \end{bmatrix}, \quad \mathcal{A}_d(:, :, 2) = \begin{bmatrix} 9 + 3i & 10 + 3i & 8 + 6i \\ 6 + 1i & 3 + 5i & 4 + 2i \\ 6 + 8i & 8 + 1i & 6 + 7i \end{bmatrix},$$

and

$$\mathcal{A}_c(:,:,1) = \begin{bmatrix} 7 & 0 - 8i & 1 - 2i \\ 8 - 4i & 2 - 4i & 9 - 2i \\ 4 - 2i & 10 - 10i & 5 - 1i \end{bmatrix}, \quad \mathcal{A}_c(:,:,2) = \begin{bmatrix} 10 - 1i & 1 - 6i & 8 - 6i \\ 0 - 9i & 10 - 1i & 8 - 3i \\ 4 - 6i & 0 - 9i & 9 - 5i \end{bmatrix}.$$

Then, applying Algorithm 1, we obtain a unitary tensor  $\mathcal{U} = \mathcal{U}_d + \mathbf{j}\mathcal{U}_c$ , where

$$\mathcal{U}_d(:,:,1) = \begin{bmatrix} 0.0977 - 0.0957i & -0.0911 + 0.2117i & 0.0162 + 0.2244i \\ -0.0457 - 0.0162i & 0.002 + 0.3894i & 0.2925 + 0.0834i \\ 0.1745 + 0.214i & 0.0278 - 0.1106i & -0.0672 - 0.2074i \end{bmatrix},$$

$$\mathcal{U}_d(:,:,2) = \begin{bmatrix} 0.1729 + 0.0002i & 0.3501 - 0.1514i & 0.1663 + 0.1022i \\ 0.1367 + 0.0786i & -0.0408 + 0.1717i & 0.206 - 0.1925i \\ 0.1029 + 0.2674i & 0.1983 - 0.1068i & 0.033 + 0.3279i \end{bmatrix},$$

and

$$\mathcal{U}_c(:,:,1) = \begin{bmatrix} 0.122 + 0.0194i & -0.1388 - 0.182i & -0.1728 - 0.0508i \\ 0.2798 + 0.0329i & -0.0719 + 0.0795i & 0.1302 + 0.0373i \\ 0.1548 + 0.022i & 0.427 - 0.2406i & -0.0389 + 0.2302i \end{bmatrix},$$

$$\mathcal{U}_c(:,:,2) = \begin{bmatrix} 0.4842 + 0.1635i & 0.0403 + 0.1116i & 0.229 - 0.4861i \\ -0.3868 - 0.4185i & 0.2866 + 0.1137i & 0.2683 - 0.1304i \\ -0.1303 - 0.2095i & -0.1532 - 0.3437i & 0.3163 - 0.0106i \end{bmatrix},$$

and a Hermitian and f-positive semidefinite tensor  $\mathcal{H} = \mathcal{H}_d + \mathbf{j}\mathcal{H}_c$ , where

$$\mathcal{H}_d(:,:,1) = \begin{bmatrix} 21.4335 & 3.0005 - 1.9322i & 9.0186 + 1.9319i \\ 3.0005 + 1.9322i & 23.4129 & 9.018 + 2.7682i \\ 9.0186 - 1.9319i & 9.018 - 2.7682i & 18.784 \end{bmatrix},$$

$$\mathcal{H}_d(:,:,2) = \begin{bmatrix} 10.3414 & 7.0911 + 0.8509i & 6.3135 + 3.4139i \\ 7.0911 - 0.8509i & 7.0046 & 9.124 + 1.3119i \\ 6.3135 - 3.4139i & 9.124 - 1.3119i & 6.554 \end{bmatrix},$$

and

$$\mathcal{H}_c(:,:,1) = \begin{bmatrix} 0 & 1.8096 - 3.7384i & 0.3446 - 0.4488i \\ -1.8096 + 3.7384i & 0 & 1.648 + 3.1267i \\ -0.3446 + 0.4488i & -1.648 - 3.1267i & 0 \end{bmatrix},$$

$$\mathcal{H}_c(:,:,2) = \begin{bmatrix} 0 & -1.2903 - 3.9939i & 0.397 - 0.9932i \\ 1.2903 + 3.9939i & 0 & -1.4261 + 2.9459i \\ -0.397 + 0.9932i & 1.4261 - 2.9459i & 0 \end{bmatrix},$$

which satisfy  $\mathcal{A} = \mathcal{U} * Q \mathcal{H}$ .

**Remark 4.6.** Similarly, we can demonstrate the left polar decomposition, that is  $\mathcal{A} = \mathcal{K} * Q \mathcal{W}$ , where  $\mathcal{W}$  is a unitary quaternion tensor and  $\mathcal{K}$  is a Hermitian and f-positive semidefinite quaternion tensor. Unless otherwise indicated, QT-Polar decomposition herein refers to the QT-Right Polar decomposition.

Based on the above remark, suppose that  $\mathcal{K} = \mathcal{U} *_Q \mathcal{S} *_Q \mathcal{U}^*$  and  $\mathcal{W} = \mathcal{U} *_Q \mathcal{V}^*$ . Then we obtain  $\mathcal{K} *_Q \mathcal{W} = \mathcal{U} *_Q \mathcal{S} *_Q \mathcal{U}^* *_Q \mathcal{U} *_Q \mathcal{V}^* = \mathcal{U} *_Q \mathcal{S} *_Q \mathcal{V}^*$ . Notice that it is a special SVD when  $\mathcal{K} *_Q \mathcal{W} \in \mathbb{Q}^{n \times n \times n_3}$ . Certainly, we also provide the general SVD as follows, which is studied in [22, Theorem 2.2]. It is worth noting that we remove an extra limitation in its proof that  $\text{diag}(\hat{\mathcal{S}})$  is diagonal and reprove the SVD of quaternion tensors.

**Corollary 4.7 (QT-SVD).** *Let  $\mathcal{A} \in \mathbb{Q}^{n_1 \times n_2 \times n_3}$ . Then there exist unitary quaternion tensors  $\mathcal{U} \in \mathbb{Q}^{n_1 \times n_1 \times n_3}$ ,  $\mathcal{V} \in \mathbb{Q}^{n_2 \times n_2 \times n_3}$ , and an f-diagonal tensor  $\mathcal{S} \in \mathbb{Q}^{n_1 \times n_2 \times n_3}$  such that  $\mathcal{A}$  can be factored as*

$$\mathcal{A} = \mathcal{U} *_Q \mathcal{S} *_Q \mathcal{V}^*.$$

Meanwhile,

$$\text{bcirc}_z(\mathcal{A}) = \text{bcirc}_z(\mathcal{U}) \text{bcirc}_z(\mathcal{S}) \text{bcirc}_z(\mathcal{V})^*,$$

where  $\text{bcirc}_z(\mathcal{U})$  and  $\text{bcirc}_z(\mathcal{V})$  are both unitary and all the entries of  $\text{bcirc}_z(\mathcal{S})$  are diagonal.

*Proof.* According to the quaternion matrix SVD, which is discussed in [32], we can construct each frontal slice of  $\hat{\mathcal{A}}$  by

$$\hat{\mathcal{A}}^{(i)} = \hat{\mathcal{U}}^{(i)} \hat{\mathcal{S}}^{(i)} (\hat{\mathcal{V}}^{(i)})^*, \quad i = 1, 2, \dots, n_3,$$

where  $\hat{\mathcal{U}}^{(i)} \in \mathbb{Q}^{n_1 \times n_1}$  and  $\hat{\mathcal{V}}^{(i)} \in \mathbb{Q}^{n_2 \times n_2}$  are both unitary, and  $\hat{\mathcal{S}}^{(i)} \in \mathbb{Q}^{n_1 \times n_2}$  is diagonal such that  $\hat{\mathcal{U}}^{(i)}$ ,  $\hat{\mathcal{V}}^{(i)}$ , and  $\hat{\mathcal{S}}^{(i)}$  is the  $i$ -th diagonal entry of  $\hat{\mathcal{U}}$ ,  $\hat{\mathcal{V}}$ , and  $\hat{\mathcal{S}}$ , respectively. Hence, we have

$$\text{diag}(\hat{\mathcal{A}}) = \text{diag}(\hat{\mathcal{U}}) \text{diag}(\hat{\mathcal{S}}) \text{diag}(\hat{\mathcal{V}})^*,$$

where  $\text{diag}(\hat{\mathcal{U}})$  and  $\text{diag}(\hat{\mathcal{V}})$  are both unitary.

By Theorem 3.2, we have

$$\text{bcirc}_z(\mathcal{U}) = (F_{n_3}^* \otimes I_n) \text{diag}(\hat{\mathcal{U}}) (F_{n_3} \otimes I_n),$$

then  $\text{bcirc}_z(\mathcal{U})$  is unitary. Furthermore, by Corollary 3.8, we obtain  $\mathcal{U}$  is unitary. Similarly,  $\mathcal{V}$  is unitary.

Using Theorem 3.2, routine calculation follows

$$\text{bcirc}_z(\mathcal{A}) = \text{bcirc}_z(\mathcal{U}) \text{bcirc}_z(\mathcal{S}) \text{bcirc}_z(\mathcal{V})^*,$$

From Theorem 3.6, we have

$$\text{bcirc}_z(\mathcal{A}) = \text{bcirc}_z(\mathcal{U}) \text{bcirc}_z(\mathcal{S}) \text{bcirc}_z(\mathcal{V}^*),$$

Applying Theorem 3.4 and equation (4), it directly follows that

$$\mathcal{A} = \mathcal{U} *_Q \mathcal{S} *_Q \mathcal{V}^*,$$

where  $\mathcal{S}$  is an f-diagonal quaternion tensor.

On the other hand, observing the structure of (6), it is obvious that all the entries of  $\text{bcirc}_z(\mathcal{S})$  are diagonal.  $\square$

**Remark 4.8.** It is worth noting that  $\mathcal{S}$  is  $f$ -diagonal equivalent to  $\hat{\mathcal{S}}$  being  $f$ -diagonal from (4). However, the proof in [22, Theorem 2.2] mentions that  $\text{diag}(\hat{\mathcal{S}})$  is diagonal. Actually, this extra limitation is not required. In what follows, we provide a numerical example to illustrate the truth.

---

**Algorithm 2** QT-SVD [18]

---

**Input:** Third-order quaternion tensor  $\mathcal{A} \in \mathbb{Q}^{n_1 \times n_2 \times n_3}$ .

**Output:** Third-order unitary quaternion tensors  $\mathcal{U} \in \mathbb{Q}^{n_1 \times n_1 \times n_3}$  and  $\mathcal{V} \in \mathbb{Q}^{n_2 \times n_2 \times n_3}$ , third-order  $f$ -diagonal quaternion tensor  $\mathcal{S} \in \mathbb{Q}^{n_1 \times n_2 \times n_3}$ .

```

1:  $\hat{\mathcal{A}} = \text{fftq}(\mathcal{A}, [ ], 3)$ 
2: for  $i = 1, 2, \dots, n_3$  do
    $[\hat{\mathcal{U}}(:, :, i), \hat{\mathcal{S}}(:, :, i), \hat{\mathcal{V}}(:, :, i)] = \text{svd}(\hat{\mathcal{A}}(:, :, i))$ 
3: end for
4:  $\mathcal{U} = \text{ifftq}(\hat{\mathcal{U}}, [ ], 3)$ ,  $\mathcal{S} = \text{ifftq}(\hat{\mathcal{S}}, [ ], 3)$ ,  $\mathcal{V} = \text{ifftq}(\hat{\mathcal{V}}, [ ], 3)$ 

```

---

**Example 4.9.** Let  $\mathcal{A} = \mathcal{A}_d + j\mathcal{A}_c \in \mathbb{Q}^{3 \times 2 \times 3}$  whose frontal slices are given below.

$$\mathcal{A}_d(:, :, 1) = \begin{bmatrix} -0.4102 - 0.201i & -0.6358 - 0.4573i \\ -0.5639 + 0.1595i & 0.4203 + 0.0335i \\ -0.6145 - 0.2805i & 0.09 - 0.6297i \end{bmatrix}, \mathcal{A}_c(:, :, 1) = \begin{bmatrix} -0.3436 - 0.8205i & 0.169 - 0.5984i \\ 0.1612 - 0.7941i & 0.4122 + 0.8077i \\ -0.4092 + 0.6133i & -0.1043 + 0.7645i \end{bmatrix},$$

$$\mathcal{A}_d(:, :, 2) = \begin{bmatrix} -0.1818 + 0.4305i & 0.3797 - 0.054i \\ 0.1108 + 0.0062i & -0.7078 + 0.1158i \\ 0.4451 + 0.1169i & 0.3098 - 0.1739i \end{bmatrix}, \mathcal{A}_c(:, :, 2) = \begin{bmatrix} -0.7455 - 0.4753i & -0.5206 - 0.7628i \\ -0.7029 + 0.7026i & -0.6927 - 0.0756i \\ 0.8874 + 0.029i & -0.3586 + 0.8632i \end{bmatrix},$$

$$\mathcal{A}_d(:, :, 3) = \begin{bmatrix} -0.4924 - 0.6509i & 0.9176 - 0.3561i \\ 0.8159 + 0.3591i & 0.4122 + 0.0498i \\ 0.3714 + 0.6064i & -0.4633 + 0.7219i \end{bmatrix}, \mathcal{A}_c(:, :, 3) = \begin{bmatrix} -0.3479 - 0.4613i & -0.12 + 0.1296i \\ 0.334 + 0.3062i & 0.4724 - 0.7775i \\ 0.599 + 0.3682i & 0.3624 + 0.3646i \end{bmatrix}.$$

In accordance with Algorithm 2 in [18], applying the  $\text{fftq}(\mathcal{A}, [ ], 3)$  operation to  $\mathcal{A}$  along the third mode yields the transformed tensor  $\hat{\mathcal{A}} = \hat{\mathcal{A}}_d + j\hat{\mathcal{A}}_c$ , where

$$\hat{\mathcal{A}}_d(:, :, 1) = \begin{bmatrix} -1.0844 - 0.4214i & 0.6615 - 0.8674i \\ 0.3629 + 0.5248i & 0.1247 + 0.1991i \\ 0.2019 + 0.4428i & -0.0635 - 0.0818i \end{bmatrix}, \hat{\mathcal{A}}_c(:, :, 1) = \begin{bmatrix} -1.437 - 1.7572i & -0.4715 - 1.2316i \\ -0.2076 + 0.2147i & 0.1918 - 0.0454i \\ 1.0771 + 1.0106i & -0.1006 + 1.9923i \end{bmatrix},$$

$$\hat{\mathcal{A}}_d(:, :, 2) = \begin{bmatrix} 0.8634 - 0.3598i & -1.0228 + 0.2136i \\ -1.3329 + 0.5874i & 0.6253 + 0.9207i \\ -1.4466 - 0.706i & -0.609 - 1.5733i \end{bmatrix}, \hat{\mathcal{A}}_c(:, :, 2) = \begin{bmatrix} 0.2152 - 0.6965i & 1.2622 - 0.6287i \\ 0.0023 - 2.1965i & -0.0855 + 0.2252i \\ -0.8586 + 0.6645i & -0.538 - 0.4738i \end{bmatrix},$$

$$\hat{\mathcal{A}}_d(:, :, 3) = \begin{bmatrix} -1.0097 + 0.1783i & -1.5461 - 0.7181i \\ -0.7216 - 0.6338i & 0.5109 - 1.0193i \\ -0.5988 - 0.5784i & 0.9425 - 0.2342i \end{bmatrix}, \hat{\mathcal{A}}_c(:, :, 3) = \begin{bmatrix} 0.1909 - 0.008i & -0.2836 + 0.0651i \\ 0.689 - 0.4005i & 1.1302 + 2.2432i \\ -1.4462 + 0.1649i & 0.3256 + 0.7749i \end{bmatrix}.$$

Then performing the SVD on each frontal slice of  $\hat{\mathcal{A}}$  to obtain  $\hat{\mathcal{U}}$ ,  $\hat{\mathcal{S}}$ , and  $\hat{\mathcal{V}}$ . The frontal slices of  $\hat{\mathcal{U}} = \hat{\mathcal{U}}_d + j\hat{\mathcal{U}}_c$  are listed below.

$$\hat{\mathcal{U}}_d(:, :, 1) = \begin{bmatrix} -0.316 - 0.2197i & 0.194 - 0.3172i & -0.022 + 0.2968i \\ 0.1119 + 0.1231i & -0.0399 - 0.2149i & -0.3006 + 0.2423i \\ 0.1197 - 0.0027i & 0.2103 - 0.613i & 0.0389 + 0.1057i \end{bmatrix},$$

$$\hat{\mathcal{U}}_d(:, :, 2) = \begin{bmatrix} 0.0741 - 0.1092i & -0.553 - 0.0001i & -0.2588 + 0.1853i \\ -0.2397 + 0.1718i & 0.4848 - 0.0189i & -0.3055 + 0.1774i \\ -0.408 - 0.2385i & 0.0908 - 0.0717i & -0.3391 + 0.2349i \end{bmatrix},$$

$$\begin{aligned}
\hat{\mathcal{U}}_{\mathbf{d}}(:,:,3) &= \begin{bmatrix} -0.3258 + 0.2581i & 0.2858 + 0.2151i & 0.1633 + 0.026i \\ -0.338 - 0.583i & 0.0651 - 0.3218i & -0.3582 - 0.3612i \\ -0.1246 - 0.3518i & 0.2604 - 0.055i & -0.0401 + 0.3709i \end{bmatrix}, \\
\hat{\mathcal{U}}_{\mathbf{c}}(:,:,1) &= \begin{bmatrix} -0.4497 - 0.4981i & 0.1318 + 0.3711i & -0.1335 + 0.0429i \\ -0.0402 + 0.019i & 0.1195 - 0.215i & -0.1106 - 0.8371i \\ 0.4208 + 0.4248i & 0.2405 + 0.3472i & -0.0494 + 0.1207i \end{bmatrix}, \\
\hat{\mathcal{U}}_{\mathbf{c}}(:,:,2) &= \begin{bmatrix} -0.0157 - 0.3168i & -0.2385 - 0.3107i & -0.0244 + 0.5664i \\ 0.0912 - 0.5875i & 0.2666 + 0.2318i & 0.0911 + 0.2573i \\ -0.3572 + 0.3011i & -0.2851 + 0.2932i & -0.4536 + 0.0441i \end{bmatrix}, \\
\hat{\mathcal{U}}_{\mathbf{c}}(:,:,3) &= \begin{bmatrix} 0.1314 - 0.2113i & 0.0384 - 0.2741i & 0.3643 + 0.633i \\ 0.2915 - 0.2155i & -0.1034 - 0.0009i & -0.0846 + 0.1732i \\ -0.1881 + 0.071i & 0.7782 - 0.0232i & 0.0456 - 0.0452i \end{bmatrix}.
\end{aligned}$$

Also, each frontal slice of  $\hat{\mathcal{V}} = \hat{\mathcal{V}}_{\mathbf{d}} + \mathbf{j}\hat{\mathcal{V}}_{\mathbf{c}}$  is listed as follows.

$$\begin{aligned}
\hat{\mathcal{V}}_{\mathbf{d}}(:,:,1) &= \begin{bmatrix} 0.7662 & 0.4201 + 0.4152i \\ -0.6426 & 0.5009 + 0.4951i \end{bmatrix}, \hat{\mathcal{V}}_{\mathbf{c}}(:,:,1) = \begin{bmatrix} 0 & 0.1618 + 0.1945i \\ 0 & 0.1929 + 0.232i \end{bmatrix}, \\
\hat{\mathcal{V}}_{\mathbf{d}}(:,:,2) &= \begin{bmatrix} 0.8947 & 0.1687 + 0.2127i \\ -0.4466 & 0.3379 + 0.4262i \end{bmatrix}, \hat{\mathcal{V}}_{\mathbf{c}}(:,:,2) = \begin{bmatrix} 0 & -0.3418 - 0.0943i \\ 0 & -0.6849 - 0.1889i \end{bmatrix}, \\
\hat{\mathcal{V}}_{\mathbf{d}}(:,:,3) &= \begin{bmatrix} 0.4792 & 0.1269 + 0.5947i \\ -0.8777 & 0.0693 + 0.3247i \end{bmatrix}, \hat{\mathcal{V}}_{\mathbf{c}}(:,:,3) = \begin{bmatrix} 0 & 0.4678 - 0.4264i \\ 0 & 0.2554 - 0.2328i \end{bmatrix}.
\end{aligned}$$

It is noteworthy that

$$diag(\hat{\mathcal{S}})(:,:) = \begin{bmatrix} 3.8889 & 0 & 0 & 0 & 0 & 0 \\ 0 & 1.1447 & 0 & 0 & 0 & 0 \\ 0 & 0 & 0 & 0 & 0 & 0 \\ 0 & 0 & 3.6848 & 0 & 0 & 0 \\ 0 & 0 & 0 & 2.5063 & 0 & 0 \\ 0 & 0 & 0 & 0 & 0 & 0 \\ 0 & 0 & 0 & 0 & 3.8902 & 0 \\ 0 & 0 & 0 & 0 & 0 & 1.604 \\ 0 & 0 & 0 & 0 & 0 & 0 \end{bmatrix},$$

which is not a diagonal matrix.

In what follows, we obtain two unitary tensors  $\mathcal{U}$ ,  $\mathcal{V}$ , and an f-diagonal tensor  $\mathcal{S}$ . Specifically, the frontal slices of  $\mathcal{U} = \mathcal{U}_{\mathbf{d}} + \mathbf{j}\mathcal{U}_{\mathbf{c}}$  are represented as

$$\begin{aligned}
\mathcal{U}_{\mathbf{d}}(:,:,1) &= \begin{bmatrix} -0.1892 - 0.0236i & -0.0244 - 0.034i & -0.0392 + 0.1694i \\ -0.1552 - 0.0961i & 0.17 - 0.1852i & -0.3215 + 0.0195i \\ -0.1376 - 0.1977i & 0.1872 - 0.2466i & -0.1134 + 0.2372i \end{bmatrix}, \\
\mathcal{U}_{\mathbf{d}}(:,:,2) &= \begin{bmatrix} 0.0426 + 0.0174i & 0.1713 - 0.3837i & -0.0374 - 0.0582i \\ -0.0843 + 0.1379i & -0.1924 + 0.1063i & -0.1451 + 0.1266i \\ 0.0959 + 0.0157i & 0.0164 - 0.2322i & 0.1154 - 0.152i \end{bmatrix}, \\
\mathcal{U}_{\mathbf{d}}(:,:,3) &= \begin{bmatrix} -0.1694 - 0.2135i & 0.0471 + 0.1006i & 0.0546 + 0.1856i \\ 0.3515 + 0.0812i & -0.0175 - 0.136i & 0.1659 + 0.0962i \\ 0.1614 + 0.1793i & 0.0068 - 0.1343i & 0.0369 + 0.0206i \end{bmatrix},
\end{aligned}$$

and

$$\mathcal{U}_{\mathbf{c}}(:,:,1) = \begin{bmatrix} -0.1113 - 0.3421i & -0.0227 - 0.0713i & 0.0688 + 0.4141i \\ 0.1142 - 0.2614i & 0.0942 + 0.0053i & -0.0347 - 0.1355i \\ -0.0415 + 0.2656i & 0.2445 + 0.2057i & -0.1525 + 0.0399i \end{bmatrix},$$

$$\mathcal{U}_c(:,:,2) = \begin{bmatrix} -0.1996 - 0.0355i & 0.0667 + 0.3011i & -0.1204 - 0.0734i \\ -0.1846 + 0.198i & 0.0798 - 0.217i & -0.0137 - 0.4015i \\ 0.2976 + 0.1284i & 0.0893 + 0.3777i & 0.0773 + 0.1845i \end{bmatrix},$$

$$\mathcal{U}_c(:,:,3) = \begin{bmatrix} -0.1388 - 0.1205i & 0.0879 + 0.1413i & -0.082 - 0.2978i \\ 0.0302 + 0.0823i & -0.0545 - 0.0034i & -0.0622 - 0.3001i \\ 0.1647 + 0.0308i & -0.0934 - 0.2362i & 0.0257 - 0.1037i \end{bmatrix}.$$

Then the frontal slices of  $\mathcal{V} = \mathcal{V}_d + j\mathcal{V}_c$  are given by

$$\mathcal{V}_d(:,:,1) = \begin{bmatrix} 0.7134 & -0.6556 \\ 0.2385 - 0.4075i & 0.3027 - 0.4153i \end{bmatrix}, \quad \mathcal{V}_c(:,:,1) = \begin{bmatrix} 0 & 0 \\ -0.0959 + 0.1087i & 0.0788 + 0.0632i \end{bmatrix},$$

$$\mathcal{V}_d(:,:,2) = \begin{bmatrix} 0.0264 + 0.12i & 0.0065 + 0.1245i \\ -0.0195 + 0.0082i & 0.1284 + 0.0377i \end{bmatrix}, \quad \mathcal{V}_c(:,:,2) = \begin{bmatrix} 0 & 0 \\ 0.0629 + 0.0821i & -0.1232 + 0.1238i \end{bmatrix},$$

$$\mathcal{V}_d(:,:,3) = \begin{bmatrix} 0.0264 - 0.12i & 0.0065 - 0.1245i \\ 0.201 - 0.0159i & 0.0698 - 0.1174i \end{bmatrix}, \quad \mathcal{V}_c(:,:,3) = \begin{bmatrix} 0 & 0 \\ -0.1288 - 0.3853i & -0.1486 - 0.419i \end{bmatrix}.$$

Note that the frontal slices of  $\mathcal{S}$  are diagonal matrices, as shown below.

$$\mathcal{S}(:,:,1) = \begin{bmatrix} 3.8213 & 0 \\ 0 & 1.7517 \\ 0 & 0 \end{bmatrix}, \quad \mathcal{S}(:,:,2) = \begin{bmatrix} 0.0338 & 0 \\ 0 & -0.3035 \\ 0 & 0 \end{bmatrix}, \quad \mathcal{S}(:,:,3) = \begin{bmatrix} 0.0338 & 0 \\ 0 & -0.3035 \\ 0 & 0 \end{bmatrix}.$$

Above all, we observe that  $\text{diag}(\hat{\mathcal{S}})$  is not a diagonal matrix. Actually,  $\text{diag}(\hat{\mathcal{S}})$  is also not required to be a diagonal matrix. In general, requiring  $\text{diag}(\hat{\mathcal{S}})$  to be diagonal and each of its frontal slices to be diagonal leaves only one possibility: the first slice of  $\text{diag}(\hat{\mathcal{S}})$  is diagonal, while all remaining slices are zero. Such a requirement is evidently too restrictive.

Moreover, the LU decomposition with permutation for quaternion matrices [28, 16] is further generalized to quaternion tensors. Before proceeding, the following definitions are provided.

**Definition 4.10 (F-Permutation Tensor).** Let  $\mathcal{A} \in \mathbb{R}^{n \times n \times n^3}$ .  $\mathcal{A}$  is called an f-permutation tensor if each frontal slice of  $\mathcal{A}$  is a permutation matrix.

**Definition 4.11 (Unit F-upper (lower)-triangular Quaternion Tensor).** The tensor  $\mathcal{P} \in \mathbb{Q}^{n \times n \times n^3}$  is called a unit f-upper (lower)-triangular quaternion tensor whose first frontal slice is a unit upper (lower)-triangular quaternion matrix and the remaining frontal slices are upper (lower)-triangular quaternion matrices.

Now, we provide a new LU decomposition with permutation of quaternion tensors via the QT-product.

**Theorem 4.12 (QT-PLU decomposition).** Let  $\mathcal{A} \in \mathbb{Q}^{n \times n \times n^3}$ . Then there exist a unit f-lower-triangular tensor  $\mathcal{L} \in \mathbb{Q}^{n \times n \times n^3}$ , an f-upper-triangular tensor  $\mathcal{U} \in \mathbb{Q}^{n \times n \times n^3}$ , and an f-permutation tensor  $\hat{\mathcal{P}}$  such that

$$\mathcal{P} *_Q \mathcal{A} = \mathcal{L} *_Q \mathcal{U}.$$

Meanwhile,

$$\text{bcirc}_z(\mathcal{P})\text{bcirc}_z(\mathcal{A}) = \text{bcirc}_z(\mathcal{L})\text{bcirc}_z(\mathcal{U}),$$

where the first diagonal entry of  $\text{bcirc}_z(\mathcal{L})$  is unit lower triangular, the remaining entries of  $\text{bcirc}_z(\mathcal{L})$  are lower triangular and all the entries of  $\text{bcirc}_z(\mathcal{U})$  are upper triangular, and all the entries of  $\text{bcirc}_z(\hat{\mathcal{P}})$  are permutation matrices.

*Proof.* Based on [28], we can construct the following equation

$$\hat{\mathcal{P}}^{(i)} \hat{\mathcal{A}}^{(i)} = \hat{\mathcal{L}}^{(i)} \hat{\mathcal{U}}^{(i)}, \quad i = 1, 2, \dots, n_3,$$

where  $\hat{\mathcal{P}}^{(i)}$  is a permutation matrix,  $\hat{\mathcal{L}}^{(i)}$  is a unit lower-triangular matrix, and  $\hat{\mathcal{U}}^{(i)}$  is an upper-triangular matrix. Let  $\hat{\mathcal{P}}^{(i)}$ ,  $\hat{\mathcal{A}}^{(i)}$ ,  $\hat{\mathcal{L}}^{(i)}$ , and  $\hat{\mathcal{U}}^{(i)}$  represent the  $i$ -th diagonal entry of  $\hat{\mathcal{P}}$ ,  $\hat{\mathcal{A}}$ ,  $\hat{\mathcal{L}}$ , and  $\hat{\mathcal{U}}$ , respectively. Thus,

$$\text{diag}(\hat{\mathcal{P}}) \text{diag}(\hat{\mathcal{A}}) = \text{diag}(\hat{\mathcal{L}}) \text{diag}(\hat{\mathcal{U}}),$$

where  $\text{diag}(\hat{\mathcal{L}})$  is a unit lower-triangular matrix,  $\text{diag}(\hat{\mathcal{U}})$  is an upper-triangular matrix, and  $\text{diag}(\hat{\mathcal{P}})$  is a permutation matrix. In addition,  $\hat{\mathcal{L}}$  is unit f-lower triangular,  $\hat{\mathcal{U}}$  is f-upper triangular, and  $\hat{\mathcal{P}}$  is an f-permutation tensor.

Utilizing Theorem 3.2, it directly follows

$$\text{bcirc}_z(\mathcal{P}) \text{bcirc}_z(\mathcal{A}) = \text{bcirc}_z(\mathcal{L}) \text{bcirc}_z(\mathcal{U}).$$

Then, by Theorem 3.4 and equation (4), a simple analysis reveals that  $\mathcal{P} *_Q \mathcal{A} = \mathcal{L} *_Q \mathcal{U}$ , where  $\mathcal{L}$  is a unit f-lower-triangular tensor, and  $\mathcal{U}$  is an f-upper-triangular tensor.

Moreover, the structure of (6) reveals that the first diagonal entry of  $\text{bcirc}_z(\mathcal{L})$  is unit lower triangular, the remaining entries of  $\text{bcirc}_z(\mathcal{L})$  are lower triangular, and all the entries of  $\text{bcirc}_z(\mathcal{U})$  are upper triangular, and all the entries of  $\text{bcirc}_z(\hat{\mathcal{P}})$  are permutation matrices.  $\square$

To compute the QT-PLU decomposition, we introduce the following algorithm.

---

### Algorithm 3 QT-PLU

---

**Input:** Third-order quaternion tensor  $\mathcal{A} \in \mathbb{Q}^{n \times n \times n_3}$

**Output:** Third-order unit f-lower-triangular tensor  $\mathcal{L} \in \mathbb{Q}^{n \times n \times n_3}$ , an f-upper-triangular tensor  $\mathcal{U} \in \mathbb{Q}^{n \times n \times n_3}$ , and a tensor  $\mathcal{P} \in \mathbb{Q}^{n \times n \times n_3}$ .

```

1:  $\hat{\mathcal{A}} = fftq(\mathcal{A}, [ ], 3)$ 
2: for  $i = 1, 2, \dots, n_3$  do
    $[\hat{\mathcal{L}}(:, :, i), \hat{\mathcal{U}}(:, :, i), \hat{\mathcal{P}}(:, :, i)] = plu(\hat{\mathcal{A}}(:, :, i))$ 
3: end for
4:  $\mathcal{L} = ifftq(\hat{\mathcal{L}}, [ ], 3)$ ,  $\mathcal{U} = ifftq(\hat{\mathcal{U}}, [ ], 3)$ ,  $\mathcal{P} = ifftq(\hat{\mathcal{P}}, [ ], 3)$ 

```

---

The following example is provided to demonstrate the accuracy of Algorithm 3 in computing the QT-PLU decomposition.

**Example 4.13.** Let  $\mathcal{A} = \mathcal{A}_d + j\mathcal{A}_c \in \mathbb{Q}^{3 \times 3 \times 2}$  with entries

$$\mathcal{A}_d(:, :, 1) = \begin{bmatrix} 5 + 1i & 0 + 5i & 7 + 6i \\ 3 + 6i & 5 + 9i & 9 + 3i \\ 5 + 9i & 0 + 5i & 9 + 7i \end{bmatrix}, \quad \mathcal{A}_d(:, :, 2) = \begin{bmatrix} 10 + 1i & 8 + 8i & 10 \\ 4 + 2i & 4 + 1i & 5 + 3i \\ 1 + 10i & 6 + 2i & 10 + 10i \end{bmatrix},$$

and

$$\mathcal{A}_c(:, :, 1) = \begin{bmatrix} 10 - 10i & 3 - 4i & 2 - 2i \\ 3 - 10i & 0 - 4i & 3 - 8i \\ 1 - 5i & 1 - 5i & 0 - 1i \end{bmatrix}, \quad \mathcal{A}_c(:, :, 2) = \begin{bmatrix} 5 - 8i & 7 - 10i & 4 - 9i \\ 4 - 3i & 4 - 10i & 9 - 3i \\ 4 - 2i & 9 - 6i & 3 - 10i \end{bmatrix}.$$

Moreover, utilizing Algorithm 3, we obtain a unit  $f$ -lower-triangular tensor  $\mathcal{L}$  an  $f$ -upper-triangular tensor  $\mathcal{U} = \mathcal{U}_d + \mathbf{j}\mathcal{U}_c$ , and a permutation tensor  $\hat{\mathcal{P}}$  and its corresponding tensor  $\mathcal{P}$  such that  $\mathcal{P} *_Q \mathcal{A} = \mathcal{L} *_Q \mathcal{U}$ . In what follows, we provide the specific forms of the aforementioned tensors.

In detail,  $\mathcal{L} = \mathcal{L}_d + \mathbf{j}\mathcal{L}_c$  is given by

$$\mathcal{L}_d(:,:,1) = \begin{bmatrix} 1 & 0 & 0 \\ 0.3159 + 0.0582i & 1 & 0 \\ 0.415 + 0.1349i & 0.1832 + 0.0981i & 1 \end{bmatrix},$$

$$\mathcal{L}_d(:,:,2) = \begin{bmatrix} 0 & 0 & 0 \\ 0.107 + 0.312i & 0 & 0 \\ 0.1762 + 0.0901i & 0.1613 + 0.2494i & 0 \end{bmatrix},$$

and

$$\mathcal{L}_c(:,:,1) = \begin{bmatrix} 0 & 0 & 0 \\ 0.0668 - 0.2169i & 0 & 0 \\ -0.0137 + 0.3521i & -0.0756 - 0.0104i & 0 \end{bmatrix},$$

$$\mathcal{L}_c(:,:,2) = \begin{bmatrix} 0 & 0 & 0 \\ 0.3355 + 0.5742i & 0 & 0 \\ 0.1654 - 0.3046i & -0.0577 + 0.0596i & 0 \end{bmatrix},$$

and  $\mathcal{U} = \mathcal{U}_d + \mathbf{j}\mathcal{U}_c$  is represented as

$$\mathcal{U}_d(:,:,1) = \begin{bmatrix} 7 + 3i & 4.5 + 10.5i & 10.5 + 3i \\ 0 & -3.7303 - 9.9293i & 7.1234 + 2.6061i \\ 0 & 0 & -2.1471 - 2.4952i \end{bmatrix},$$

$$\mathcal{U}_d(:,:,2) = \begin{bmatrix} 8 - 1i & 3.5 + 2.5i & 6.5 + 3i \\ 0 & 10.1802 - 0.7352i & 5.392 - 1.0058i \\ 0 & 0 & 3.4761 - 4.0415i \end{bmatrix},$$

and

$$\mathcal{U}_c(:,:,1) = \begin{bmatrix} 7 - 12.5i & 3 - 4i & 0 - 8i \\ 0 & 2.3395 - 0.3825i & -0.5505 + 0.0578i \\ 0 & 0 & 7.9589 + 3.1849i \end{bmatrix},$$

$$\mathcal{U}_c(:,:,2) = \begin{bmatrix} 8 - 5.5i & 7 - 10i & 6 - 3i \\ 0 & 10.041 - 9.084i & 0.3898 - 12.6735i \\ 0 & 0 & 6.8615 - 4.1623i \end{bmatrix}.$$

In addition,  $\mathcal{P}$  and  $\hat{\mathcal{P}}$  are expressed as

$$\mathcal{P}(:,:,1) = \begin{bmatrix} 0.5 & 0.5 & 0 \\ 0.5 & 0 & 0.5 \\ 0 & 0.5 & 0.5 \end{bmatrix}, \quad \mathcal{P}(:,:,2) = \begin{bmatrix} 0.5 & -0.5 & 0 \\ -0.5 & 0 & 0.5 \\ 0 & 0.5 & -0.5 \end{bmatrix},$$

and

$$\hat{\mathcal{P}}(:,:,1) = \begin{bmatrix} 1 & 0 & 0 \\ 0 & 0 & 1 \\ 0 & 1 & 0 \end{bmatrix}, \quad \hat{\mathcal{P}}(:,:,2) = \begin{bmatrix} 0 & 1 & 0 \\ 1 & 0 & 0 \\ 0 & 0 & 1 \end{bmatrix}.$$

Similarly, the following LU decomposition can be obtained.

**Theorem 4.14 (QT-LU decomposition).** *Let  $\mathcal{A} \in \mathbb{Q}^{n \times n \times n_3}$ . Then there exist a unit f-lower-triangular tensor  $\mathcal{L} \in \mathbb{Q}^{n \times n \times n_3}$  and an f-upper-triangular tensor  $\mathcal{U} \in \mathbb{Q}^{n \times n \times n_3}$  such that*

$$\mathcal{A} = \mathcal{L} *_Q \mathcal{U}.$$

Meanwhile,

$$\text{bcirc}_z(\mathcal{A}) = \text{bcirc}_z(\mathcal{L})\text{bcirc}_z(\mathcal{U}),$$

where the first diagonal entry of  $\text{bcirc}_z(\mathcal{L})$  is unit lower triangular, the remaining entries of  $\text{bcirc}_z(\mathcal{L})$  are lower triangular and all the entries of  $\text{bcirc}_z(\mathcal{U})$  are upper triangular.

*Proof.* According to [16], we can construct the following equation

$$\hat{\mathcal{A}}^{(i)} = \hat{\mathcal{L}}^{(i)}\hat{\mathcal{U}}^{(i)}, \quad i = 1, 2, \dots, n_3,$$

where  $\hat{\mathcal{L}}^{(i)}$  is a unit lower-triangular matrix and  $\hat{\mathcal{U}}^{(i)}$  is an upper-triangular matrix. Let  $\hat{\mathcal{A}}^{(i)}$ ,  $\hat{\mathcal{L}}^{(i)}$ , and  $\hat{\mathcal{U}}^{(i)}$  represent the  $i$ -th diagonal entry of  $\hat{\mathcal{A}}$ ,  $\hat{\mathcal{L}}$ , and  $\hat{\mathcal{U}}$ , respectively. Thus,

$$\text{diag}(\hat{\mathcal{A}}) = \text{diag}(\hat{\mathcal{L}})\text{diag}(\hat{\mathcal{U}}),$$

where  $\text{diag}(\hat{\mathcal{L}})$  is a unit lower-triangular matrix and  $\text{diag}(\hat{\mathcal{U}})$  is an upper-triangular matrix. In addition,  $\hat{\mathcal{L}}$  is unit f-lower triangular and  $\hat{\mathcal{U}}$  is f-upper triangular.

Utilizing Theorem 3.2, it directly follows

$$\text{bcirc}_z(\mathcal{A}) = \text{bcirc}_z(\mathcal{L})\text{bcirc}_z(\mathcal{U}).$$

Then, by Theorem 3.4 and equation (4), a simple analysis reveals that  $\mathcal{A} = \mathcal{L} *_Q \mathcal{U}$ , where  $\mathcal{L}$  is a unit f-lower-triangular tensor, and  $\mathcal{U}$  is an f-upper-triangular tensor.

Moreover, the structure of (6) reveals that the first diagonal entry of  $\text{bcirc}_z(\mathcal{L})$  is unit lower triangular, the remaining entries of  $\text{bcirc}_z(\mathcal{L})$  are lower triangular, and all the entries of  $\text{bcirc}_z(\mathcal{U})$  are upper triangular.  $\square$

We now present the algorithm for the QT-LU decomposition as follows.

---

#### Algorithm 4 QT-LU

---

**Input:** Third-order quaternion tensor  $\mathcal{A} \in \mathbb{Q}^{n \times n \times n_3}$

**Output:** Third-order unit f-lower-triangular tensor  $\mathcal{L} \in \mathbb{Q}^{n \times n \times n_3}$ , an f-upper-triangular tensor  $\mathcal{U} \in \mathbb{Q}^{n \times n \times n_3}$ .

```

1:  $\hat{\mathcal{A}} = fftq(\mathcal{A}, [ ], 3)$ 
2: for  $i = 1, 2, \dots, n_3$  do
    $[\hat{\mathcal{L}}(:, :, i), \hat{\mathcal{U}}(:, :, i)] = lu(\hat{\mathcal{A}}(:, :, i))$ 
3: end for
4:  $\mathcal{L} = ifftq(\hat{\mathcal{L}}, [ ], 3)$ ,  $\mathcal{U} = ifftq(\hat{\mathcal{U}}, [ ], 3)$ 

```

---

## 5. Large-scale experiments and Scalability analysis

This chapter presents a series of large-scale tests and scalability analysis, some of which compare the performance of the proposed algorithms with several alternative methods. All computations were performed in MATLAB R2022b using the QTFM quaternion toolbox and the Tensorlab package, and executed on a machine equipped with a 13th Gen Intel(R) Core(TM) i5-13500HX (2.50 GHz) processor and 16 GB of RAM.

We first propose the  $z$ -block circulant structure-accelerated inversion algorithm ( $\text{bcirc}_z$ -inv) to solve the problem of computing the inverse of a  $z$ -block circulant matrix. For comparison, the built-in quaternion matrix inverse function `inv` from the *MATLAB* toolbox *QTFM* is employed.

**Example 5.1.** Let  $A \in \mathbb{Q}^{n_1 n_3 \times n_1 n_3}$  be a  $z$ -block circulant matrix  $\text{bcirc}_z(\mathcal{A})$ . The inverse of  $A$  is computed through the following procedure.

1. Apply the operator  $\text{bcirc}_z^{-1}$  to  $A$  to obtain a third-order quaternion tensor

$$\mathcal{A} = \text{bcirc}_z^{-1}(A) \in \mathbb{Q}^{n_1 \times n_1 \times n_3}.$$

2. Perform the quaternion tensor Fourier transform along the third mode:

$$\widehat{\mathcal{A}} = \text{fftq}(\mathcal{A}, [ ], 3).$$

3. Compute the inverse of each frontal slice of  $\widehat{\mathcal{A}}$ , and denote the resulting tensor by  $\widehat{\mathcal{A}}^{-1}$ .
4. Apply the inverse quaternion tensor Fourier transform:

$$\mathcal{A}^{-1} = \text{ifftq}(\widehat{\mathcal{A}}^{-1}).$$

5. Finally, apply the  $\text{bcirc}_z$  operator to  $\mathcal{A}^{-1}$  to obtain the inverse matrix

$$A^{-1} = \text{bcirc}_z(\mathcal{A}^{-1}).$$

To verify the effectiveness of the proposed method, we generate a quaternion  $z$ -block circulant matrix and compute its inverse. The elements in the first column of the quaternion  $z$ -block circulant matrix are randomly generated from a uniform distribution using the `randq` function provided by the *MATLAB* toolbox *QTFM*. For each matrix dimension, the computational time is recorded and reported in Table 1.

The accuracy of the computed inverse is evaluated by measuring the distance between the product of the quaternion  $z$ -block circulant matrix and its inverse and the identity matrix, which is defined as

$$\text{err} = \max \{ \|AB - I\|, \|BA - I\| \}. \quad (16)$$

Here,  $\|\cdot\|$  denotes the Frobenius norm of a quaternion matrix, and the matrix  $B$  denotes the inverse matrix computed by the corresponding computational method. Recall that the proposed fast method is referred to as the  $\text{bcirc}_z$ -inv, while the method based on the built-in inverse function is denoted by `inv` in Table 1.

The results presented in Table 1 clearly demonstrate the computational efficiency and numerical accuracy of the proposed  $\text{bcirc}_z$ -inv method compared with the conventional quaternion matrix inverse function `inv` provided by the *QTFM* toolbox.

Table 1: Performance Comparison of  $A^{-1}$  Computation for Different Matrix Sizes

size ( $n_1 n_3 \times n_1 n_3$ )	time (s)		err	
	<b>bcirc<sub>z</sub>-inv</b>	inv	<b>bcirc<sub>z</sub>-inv</b>	inv
9 × 9	0.0096	0.0015	1.32e − 15	2.22e − 14
15 × 15	0.0043	0.0025	8.61e − 15	8.37e − 15
45 × 45	0.0091	0.0076	7.23e − 15	2.14e − 13
75 × 75	0.0126	0.0163	9.31e − 14	7.55e − 13
225 × 225	0.0456	0.0460	6.19e − 13	2.73e − 11
1125 × 1125	0.2062	0.5183	1.38e − 12	1.56e − 09
1875 × 1875	0.5017	1.4846	1.65e − 11	1.47e − 08
2500 × 2500	0.7693	2.9866	4.36e − 11	1.04e − 07
3750 × 3750	1.5859	8.6190	3.05e − 11	7.84e − 08
5000 × 5000	3.0237	18.9334	2.24e − 10	3.87e − 07

In terms of computational efficiency, the **bcirc<sub>z</sub>-inv** method exhibits significantly lower time costs as the matrix size increases. For smaller matrix sizes (e.g., 9 × 9), the built-in **inv** function is slightly faster; however, once the matrix size exceeds 75 × 75, the **bcirc<sub>z</sub>-inv** method consistently outperforms it. Moreover, the performance gap widens substantially at larger scales. For example, for a 5000 × 5000 matrix, the **bcirc<sub>z</sub>-inv** method requires only 3.02 seconds, whereas the **inv** function takes 18.93 seconds, corresponding to an 84% reduction in runtime. These results clearly demonstrate the scalability of the proposed Fourier-based approach, which exploits the block-circulant structure to significantly reduce the computational complexity.

Regarding numerical accuracy, the **bcirc<sub>z</sub>-inv** method also demonstrates superior numerical stability. Across all tested matrix sizes, the error values—measured as the deviation from the identity matrix—are consistently lower than those obtained using the **inv** method, often by several orders of magnitude. For instance, for a 2500 × 2500 matrix, the error of the **bcirc<sub>z</sub>-inv** method is  $4.36 \times 10^{-11}$ , whereas the **inv** method yields an error of  $1.04 \times 10^{-7}$ . These results indicate that the proposed method maintains higher numerical precision, particularly for large-scale problems, where numerical errors are more likely to accumulate.

In summary, the **bcirc<sub>z</sub>-inv** method provides an efficient, numerically stable, and scalable framework for computing the inverse of **bcirc<sub>z</sub>(·)**. These advantages make the proposed approach particularly well-suited for high-dimensional quaternion-valued computations, with potential applications in areas such as signal processing, computer graphics, and robotics.

To assess the computational behavior and scalability of the proposed QT-Polar decomposition (Algorithm 1), we carry out a series of evaluations on tensors of different dimensions. The comparative results are summarized in the Table 2.

**Example 5.2.** The performance analysis of the proposed QT-Polar decomposition for tensors of different dimensions indicates a consistent relationship between computational cost and numerical accuracy.

Let  $\mathcal{A} \in \mathbb{Q}^{n \times n \times n_3}$ . As the dimension of the tensor  $\mathcal{A}$  increases, the computation time increases steadily, ranging from 0.0262 seconds for the smallest 5 × 5 × 5 tensor to 373.0626 seconds for the largest 300 × 300 × 100 tensor. More significantly, the residual error remains highly stable across

all tensor dimensions, maintaining an exceptionally low level from  $2.3631 \times 10^{-14}$  for the  $5 \times 5 \times 5$  tensor to  $8.6245 \times 10^{-10}$  for the  $300 \times 300 \times 100$  tensor.

This trend indicates that the algorithm preserves high numerical precision even for large-scale tensors, with the residual error increasing only gradually by approximately four orders of magnitude as the tensor size grows by several orders of magnitude. The consistent maintenance of low residual errors across all tested configurations highlights the strong numerical stability of the proposed QT-Polar decomposition, indicating its suitability for applications requiring high-precision quaternion tensor computations.

Table 2: Performance of the proposed QT-Polar decomposition for different tensor sizes

Size of $\mathcal{A}$	Time (s)	Residual Error
$5 \times 5 \times 5$	0.0262	$2.3631 \times 10^{-14}$
$5 \times 5 \times 20$	0.1199	$4.9914 \times 10^{-14}$
$5 \times 5 \times 50$	0.2516	$8.6008 \times 10^{-14}$
$5 \times 5 \times 100$	0.5007	$1.2792 \times 10^{-13}$
$20 \times 20 \times 5$	0.0956	$3.4114 \times 10^{-13}$
$20 \times 20 \times 20$	0.3809	$8.5482 \times 10^{-13}$
$20 \times 20 \times 50$	0.9557	$1.3154 \times 10^{-12}$
$20 \times 20 \times 100$	1.8294	$1.7018 \times 10^{-12}$
$50 \times 50 \times 5$	0.3274	$2.1320 \times 10^{-12}$
$50 \times 50 \times 20$	1.1800	$6.3505 \times 10^{-12}$
$50 \times 50 \times 50$	2.8643	$8.3917 \times 10^{-12}$
$50 \times 50 \times 100$	6.0996	$1.2741 \times 10^{-11}$
$150 \times 150 \times 5$	2.8986	$3.6869 \times 10^{-11}$
$150 \times 150 \times 20$	10.5818	$6.6374 \times 10^{-11}$
$150 \times 150 \times 50$	26.8217	$1.1123 \times 10^{-10}$
$150 \times 150 \times 100$	53.2343	$1.6079 \times 10^{-10}$
$300 \times 300 \times 5$	15.6811	$1.4235 \times 10^{-10}$
$300 \times 300 \times 20$	61.4296	$3.0754 \times 10^{-10}$
$300 \times 300 \times 50$	169.2669	$4.9957 \times 10^{-10}$
$300 \times 300 \times 100$	373.0626	$8.6245 \times 10^{-10}$

Finally, a scalability analysis was performed, with the corresponding results shown in Figure 1. The figure characterizes the relationship between computational efficiency and numerical error of Algorithm 1 on the tensor size.

It is known that the tensor decomposition critically depends on the underlying matrix factorization, then variations in the matrix algorithms may lead to different decomposition outcomes. Subsequently, we examine the influence of different quaternion matrix PLU algorithms on the resulting QT-PLU tensor decomposition.

**Example 5.3.** Let  $\mathcal{A} \in \mathbb{Q}^{n \times n \times n^3}$ . To evaluate this effect, we compare three methods: the `lu` function in the MATLAB `qtfm` toolbox, Algorithm 4 in [16], and Algorithm 3.1 in [28]. The performance comparison of the three PLU decomposition algorithms over different tensor sizes exhibits clear trends in both computational efficiency and numerical accuracy. Table 3 summarizes the comparison results.

With respect to computational efficiency, Algorithm 3.1 in [28] is generally the most efficient, achieving the shortest execution times in almost all tested configurations. However, for the largest

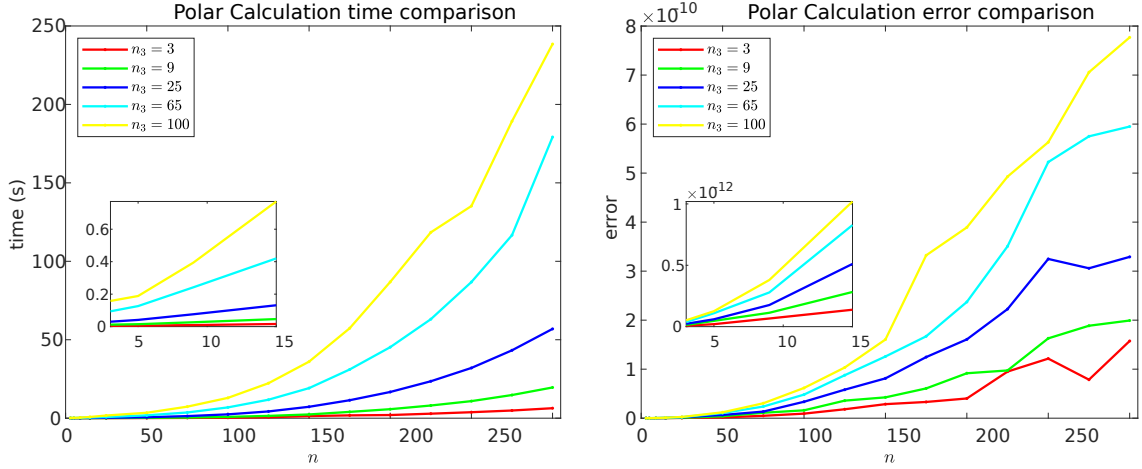


Figure 1: Performance Analysis of Polar Decomposition Algorithm

tensor size,  $300 \times 300 \times 100$ , its runtime exceeds that of Algorithm 4 in [16]—41.30 seconds versus 33.59 seconds. This observation may indicate reduced scalability of Algorithm 3.1 when applied to high-dimensional tensors. In contrast, the QTFM-LU method is consistently the slowest across all tested configurations.

In terms of numerical accuracy, Algorithm 4 in [16] shows a clear advantage, yielding the smallest residual errors in all test cases and suggesting better numerical stability. The residual errors grow predictably as the tensor dimensions increase, ranging from approximately  $10^{-15}$  for the lowest-dimensional tensors to about  $10^{-11}$  for the largest-dimensional ones.

This systematic analysis provides practical guidance for algorithm selection. Algorithm 3.1 in [28] is generally preferable for most computational scenarios, due to its clear computational advantage. Whereas Algorithm 4 in [16] is recommended when numerical accuracy is the primary concern, despite its higher computational cost. Moreover, considering both aspects, the QTFM-LU method is not recommended, even though it achieves slightly better numerical accuracy than Algorithm 4 at the smallest tensor dimensions.

For higher tensor dimensions, whether Algorithm 3.1 in [28] exhibits exponential growth in runtime remains an open question and warrants further investigation.

We also perform a scalability analysis, and the results are shown in Figure 2. The figure illustrates how the tensor dimensions affect both the computational efficiency and the numerical errors of Algorithm 3.

## 6. Applications in Tikhonov-Regularized Model and Video Rotation

In this section, large-scale testing and comparison of the Tikhonov-regularized model are performed using Theorem 3.4 and the algorithm `bcircz-inv`. Subsequently, a practical example is provided to demonstrate video rotation via the quaternion tensor polar decomposition.

Tikhonov regularization is a basic technique for solving ill-posed inverse problems by introducing a penalty term to stabilize the solution. Firstly, we describe the mathematical formulation of Tikhonov regularization in the quaternion domain, which is particularly useful for multidimensional signal processing applications, such as color image restoration and vector field analysis.

Table 3: Performance comparison of PLU decomposition algorithms for different tensor sizes

Size of $\mathcal{A}$ $n \times n \times n_3$	Computation Time (s)			Residual Error		
	QTFM-LU	Alg4 in [16]	Alg3.1 in [28]	QTFM-LU	Alg4 in [16]	Alg3.1 in [28]
$5 \times 5 \times 5$	0.01215	0.003284	<b>0.002336</b>	<b>3.8601e-15</b>	3.8633e-15	4.3505e-15
$5 \times 5 \times 20$	0.01837	0.007458	<b>0.005831</b>	9.3066e-15	<b>9.2600e-15</b>	1.0439e-14
$5 \times 5 \times 50$	0.03705	0.01191	<b>0.007119</b>	2.0122e-14	<b>1.9485e-14</b>	2.0532e-14
$5 \times 5 \times 100$	0.07474	0.02425	<b>0.01207</b>	3.1807e-14	<b>3.1650e-14</b>	3.1974e-14
$20 \times 20 \times 5$	0.01858	0.007142	<b>0.003791</b>	3.9131e-14	<b>3.8113e-14</b>	4.1009e-14
$20 \times 20 \times 20$	0.06571	0.01562	<b>0.006432</b>	8.7713e-14	<b>8.7161e-14</b>	9.2173e-14
$20 \times 20 \times 50$	0.1401	0.03569	<b>0.01454</b>	1.7556e-13	<b>1.7419e-13</b>	1.8186e-13
$20 \times 20 \times 100$	0.291	0.07754	<b>0.03346</b>	2.6913e-13	<b>2.6736e-13</b>	2.7392e-13
$50 \times 50 \times 5$	0.0439	0.01200	<b>0.005618</b>	1.9955e-13	<b>1.9897e-13</b>	2.1235e-13
$50 \times 50 \times 20$	0.1792	0.04574	<b>0.02385</b>	4.6154e-13	<b>4.5447e-13</b>	4.8628e-13
$50 \times 50 \times 50$	0.495	0.1382	<b>0.0684</b>	9.0337e-13	<b>9.0222e-13</b>	9.3352e-13
$50 \times 50 \times 100$	1.357	0.7427	<b>0.6279</b>	1.3731e-12	<b>1.3678e-12</b>	1.4074e-12
$150 \times 150 \times 5$	0.2991	0.09290	<b>0.05419</b>	1.7839e-12	<b>1.7653e-12</b>	1.8669e-12
$150 \times 150 \times 20$	1.375	0.5676	<b>0.4145</b>	3.8275e-12	<b>3.8001e-12</b>	3.9937e-12
$150 \times 150 \times 50$	4.024	1.969	<b>1.600</b>	7.3953e-12	<b>7.3514e-12</b>	7.6004e-12
$150 \times 150 \times 100$	10.26	5.971	<b>5.267</b>	1.0922e-11	<b>1.0876e-11</b>	1.1201e-11
$300 \times 300 \times 5$	1.725	0.9331	<b>0.4411</b>	7.1045e-12	<b>7.0556e-12</b>	7.4097e-12
$300 \times 300 \times 20$	7.238	4.083	<b>2.179</b>	1.5287e-11	<b>1.5186e-11</b>	1.5866e-11
$300 \times 300 \times 50$	20.72	12.90	<b>7.976</b>	2.8208e-11	<b>2.8047e-11</b>	2.8952e-11
$300 \times 300 \times 100$	50.83	<b>33.596</b>	41.30	4.2082e-11	<b>4.1860e-11</b>	4.3077e-11

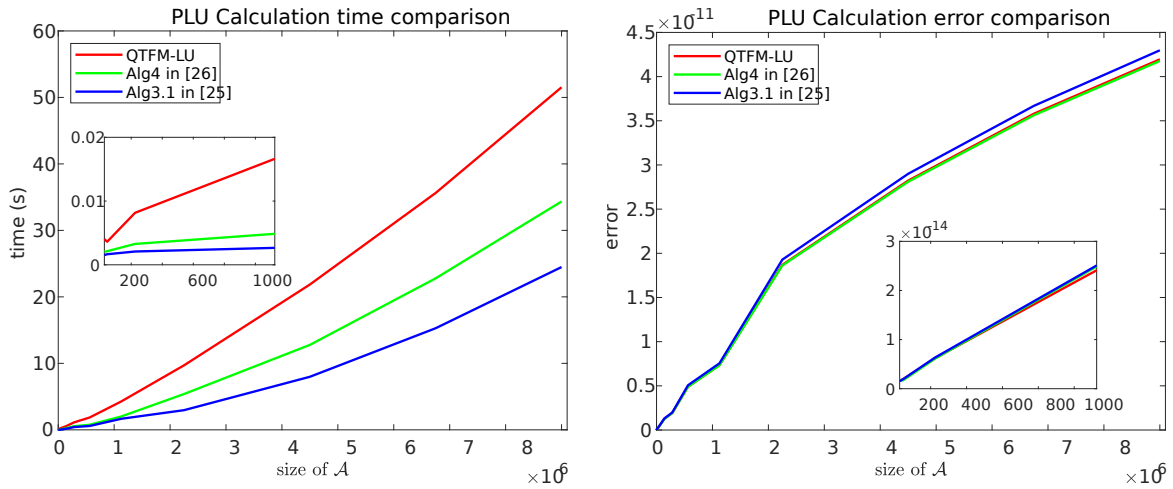


Figure 2: Performance Analysis of PLU Decomposition Algorithm

**Example 6.1.** Consider a linear inverse problem in which a quaternion matrix represents the forward operator. Let  $\mathbf{B} \in \mathbb{Q}^{n \times n}$  denote the system matrix,  $\mathbf{x} \in \mathbb{Q}^n$  the unknown signal vector, and  $\mathbf{b} \in \mathbb{Q}^n$  the observed data vector. The forward model is given by

$$\mathbf{b} = \mathbf{B}\mathbf{x} + \boldsymbol{\eta},$$

where  $\boldsymbol{\eta} \in \mathbb{Q}^n$  represents additive noise.

To address the ill-posedness of the inverse problem, we employ the classical Tikhonov regularization approach. The regularized solution is obtained by minimizing the following objective function:

$$\min_{\mathbf{x}} \left\{ \|\mathbf{B}\mathbf{x} - \mathbf{b}\|_2^2 + \lambda^2 \|\mathbf{x}\|_2^2 \right\}, \quad (17)$$

where  $\lambda > 0$  is the regularization parameter that balances the trade-off between data fidelity (the first term) and solution regularization (the second term).

The minimization problem in (17) admits a closed-form solution by setting the gradient of the objective function to zero. Expanding the objective function yields

$$J(\mathbf{x}) = (\mathbf{B}\mathbf{x} - \mathbf{b})^H(\mathbf{B}\mathbf{x} - \mathbf{b}) + \lambda^2 \mathbf{x}^H \mathbf{x}.$$

Taking the gradient with respect to  $\mathbf{x}$  and setting it to zero yields

$$\nabla_{\mathbf{x}} J(\mathbf{x}) = 2\mathbf{B}^H(\mathbf{B}\mathbf{x} - \mathbf{b}) + 2\lambda^2 \mathbf{x} = \mathbf{0}.$$

Rearranging terms leads to the associated normal equation

$$(\mathbf{B}^H \mathbf{B} + \lambda^2 \mathbf{I}) \mathbf{x} = \mathbf{B}^H \mathbf{b}.$$

Consequently, the solution can be expressed explicitly as

$$\mathbf{x}_{\text{direct}} = (\mathbf{B}^H \mathbf{B} + \lambda^2 \mathbf{I})^{-1} \mathbf{B}^H \mathbf{b}.$$

Although the direct matrix inversion method provides an exact solution to the Tikhonov regularized system, its computational complexity of  $\mathcal{O}(n^3)$  becomes prohibitive for large-scale testing, therefore practical only for small- to moderate-scale problems.

The motivation is to introduce the system matrix  $\mathbf{B}$  that possesses a  $z$ -block circulant structure  $\text{bcirc}_z(\mathcal{B})$  and exploit this special algebraic structure to accelerate the computation of the matrix inverse, thereby making large-scale experimental evaluations of the Tikhonov-regularized system using direct methods feasible. Given that

$$\mathbf{B}^H \mathbf{B} + \lambda^2 \mathbf{I} = \text{bcirc}_z(\mathcal{B}^H *_Q \mathcal{B} + \lambda^2 \mathcal{I}),$$

which is obtained by Theorem 3.4 and inherits the  $z$ -block circulant structure. Then we can compute its inverse efficiently using Example 5.1.

The computational efficiency and numerical accuracy of the algorithm  $\text{bcirc}_z\text{-inv}$  were evaluated through comprehensive numerical experiments. The algorithm was implemented in MATLAB and tested on a range of problem sizes, with its performance compared against  $\text{inv}$ .

Experiments were conducted with various tensor dimensions, where the parameter  $m$  represents the block size and  $q$  denotes the number of channels. For simplicity, let  $\mathbf{A} = \mathbf{B}^H \mathbf{B} + \lambda^2 \mathbf{I} \in \mathbb{Q}^{n \times n}$ ,

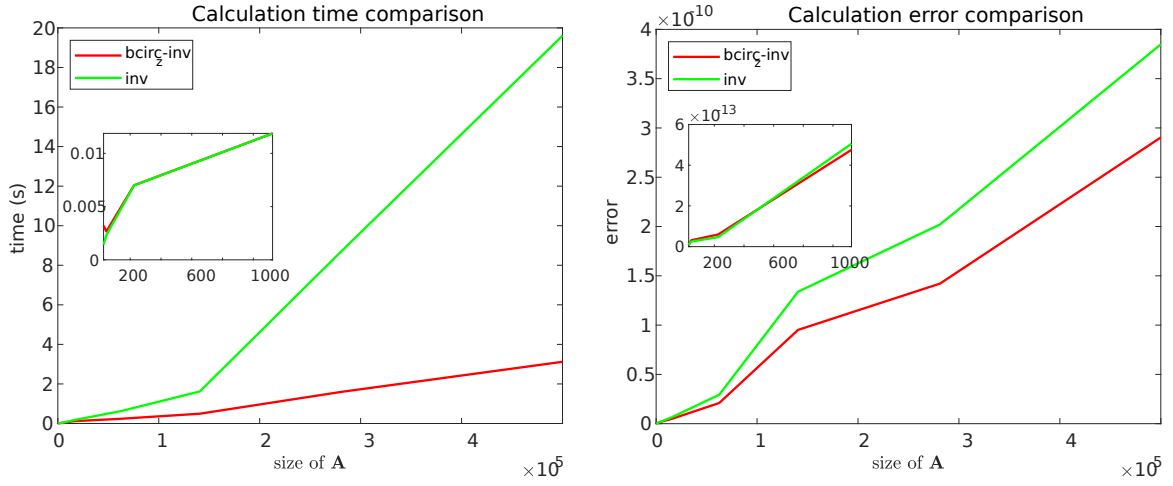


Figure 3: Scalability analysis of computing  $\mathbf{A}^{-1}$  with two methods

where  $n = mq$ . And  $\lambda = 0.5$  was used as the regularization parameter. The execution times and errors for both  $\text{bcirc}_z\text{-inv}$  and  $\text{inv}$  are presented in Fig. 3.

For small-scale testing, both methods perform comparably, with  $\text{inv}$  occasionally running slightly faster due to its lower overhead. However, as the testing size increases,  $\text{bcirc}_z\text{-inv}$  demonstrates significantly superior scaling behavior. At moderate problem sizes ( $n = 225$ ),  $\text{bcirc}_z\text{-inv}$  begins to show measurable advantages, achieving execution times approximately 20% faster than those of  $\text{inv}$ . This performance gap widens substantially as the problem dimension increases. Despite the computational acceleration,  $\text{bcirc}_z\text{-inv}$  maintains comparable numerical accuracy. The residual norms of both methods are on the order of  $10^{-11}$  to  $10^{-14}$  for smaller problems and  $10^{-10}$  to  $10^{-11}$  for larger ones. In the largest case ( $n = 5000$ ),  $\text{bcirc}_z\text{-inv}$  yields a residual of  $2.90 \times 10^{-10}$ , which is still slightly lower than the  $3.85 \times 10^{-10}$  obtained by  $\text{inv}$ . The performance gain stems from exploiting the  $z$ -block circulant structure, which reduces the computational complexity from  $\mathcal{O}(n^3)$  ( $\text{inv}$ ) to  $\mathcal{O}(m^3q + m^2q^2)$  ( $\text{bcirc}_z\text{-inv}$ ), where  $n = m \times q$ .

In summary,  $\text{bcirc}_z\text{-inv}$  exploits the special algebraic structure of the system matrix to achieve computational efficiency while maintaining numerical accuracy. This approach reduces the overall computational cost and enables the efficient solution of large-scale testing. Therefore, breaking the  $\text{inv}$  limitation to small- to moderate-scale testing. For problems with a  $z$ -block circulant structure and large dimensions,  $\text{bcirc}_z\text{-inv}$  provides a practical and efficient solution to the Tikhonov-regularized inverse problem, making it suitable for applications in color image processing and multi-channel signal analysis.

Polar decomposition has been widely applied in continuum mechanics and quantum mechanics, specifically in computer graphics, such as image rotation [25], face recognition [7], and image watermarking [35].

**Example 6.2.** In essence, the polar decomposition factors a shear-scaling matrix into the product of a rotation matrix and a scaling matrix. For matrices over the complex field, this corresponds to expressing a matrix as the product of a unitary matrix and a positive definite Hermitian matrix. In this framework, the unitary (or rotation) matrix  $Q$  captures the global rotational component, whereas the positive definite Hermitian matrix  $H$  characterizes the anisotropic scaling along the principal directions determined by its eigenvectors.

Due to its decomposition property that the polar decomposition separates deformation into pure rotation and pure scaling, we extend its application to quaternion tensors to handle the problems of video rotation, which allows for rotating different RGB channels by different angles at different frames of a video.

It is worth noting that video rotation is not only a correction tool but also a means of creative expression. In science fiction or horror films, rotating different color channels to varying degrees can depict a character's sense of loss in an alternate dimension or gravity. Traditional glitch art often involves misalignment of color channels. However, upgrading this misalignment from simple translation to rotation makes the glitch effect more dynamic and complex, no longer a cold digital error but with an organic, vortex-like texture. This technique is widely used in cyberpunk-themed films, music videos (especially electronic music, psychedelic rock), and artistic short films depicting dreams.

In what follows, we introduce an application example of using polar decomposition for video rotation. Given a rotation-scaling tensor  $\mathcal{C} \in \mathbb{Q}^{2 \times 2 \times p}$ , we use QT-polar decomposition to obtain  $\mathcal{C} = \mathcal{U} *_{\mathcal{Q}} \mathcal{H}$ , where  $\mathcal{U}$  is a unitary tensor, and  $\mathcal{H}$  is a Hermitian and  $f$ -positive semidefinite tensor. The resulting  $\mathcal{U}$  is a tensor containing rotation information for the  $R$ ,  $G$ , and  $B$  channels of the video

We apply  $\hat{\mathcal{U}}^{(n)} = \text{qfft}(\mathcal{U}^{(n)}, [ ], 3)$ , for  $n = 1, 2, \dots, p$ ,

$$\hat{\mathcal{U}}^{(n)} = \begin{pmatrix} \cos \alpha_n & 0 \\ 0 & \cos \gamma_n \end{pmatrix} i + \begin{pmatrix} \sin \alpha_n \cos \beta_n & 0 \\ 0 & \sin \gamma_n \cos \beta_n \end{pmatrix} j + \begin{pmatrix} \sin \alpha_n \sin \beta_n & 0 \\ 0 & \sin \gamma_n \sin \beta_n \end{pmatrix} k$$

Thus, by obtaining the rotation parameters  $\alpha, \beta, \gamma$ , we conducted experiments in which the  $R$ ,  $G$ , and  $B$  channels of different video frames were rotated using both identical and distinct angles, thereby producing a rotated video. The specific results are presented in Table 4.

For quantitative evaluation, we adopt the following metrics. Specifically, we compute the mean Temporal Consistency ( $TC_{mean}$ ), the mean Color Consistency ( $CC_{mean}$ ), and the standard deviation of Temporal Consistency ( $TC_{std}$ ), which are defined as follows.

$$\begin{aligned} TC_{mean} &= \frac{1}{N-1} \sum_{i=1}^{N-1} \left[ 1 - \frac{\mathbb{E}[|\mathcal{G}_{i+1} - \mathcal{G}_i|]}{255} \right], \\ CC_{mean} &= \frac{1}{N} \sum_{i=1}^N \frac{1}{1 + \bar{\sigma}_i/255}, \\ TC_{std} &= \sqrt{\frac{1}{N-2} \sum_{i=1}^{N-1} (TC_i - TC_{mean})^2}, \end{aligned}$$

where  $\mathcal{G}_i$  denotes the grayscale image of the  $i$ -th frame,  $\mathbb{E}[\cdot]$  represents the mathematical expectation (i.e., the mean),  $\bar{\sigma}_i$  is the average standard deviation of the three color channels of the  $i$ -th frame, and  $N$  denotes the frame rate of the video. The evaluation results are summarized in Table 5.

By testing several different rotation methods, we observe two key aspects: (1) The data in the temporal consistency standard deviation of the metrics also achieves favorably, which demonstrates the stability of the QT-polar decomposition. (2) The data in both temporal consistency mean and color consistency mean perform favorably, which demonstrates that the QT-polar decomposition preserves frame-to-frame coherence while maintaining stability and faithful color reproduction.

Table 4: Comparison of Image Rotation Results

frame Rotation method	120 image	120 Angle	230 image	230 Angle	340 image	340 Angle
Original		0 0 0		0 0 0		0 0 0
Same linearity <sup>a</sup>		119 119 119		220 229 229		339 339 339
Different linearity <sup>b</sup>		119 144 169		131 74 81		21 3 28
Fixed step <sup>c</sup>		119 142.8 166.6		131 94.8 39.4		21 46.8 114.6
Sine wave phase <sup>d</sup>		167.2 198.1 30.9		114.2 358.0 68.0		67.2 182.1 115.0
Logarithmic growth <sup>e</sup>		178.2 74.3 42.2		101.3 316.1 9.3		50.0 0.2 48.1

<sup>a</sup> Each channel rotates through a fixed range with constant angular velocity. And each color channel has the same initial angle.

<sup>b</sup> Each channel rotates through a fixed range with constant angular velocity. And each color channel has a different initial angle.

<sup>c</sup> Each channel rotates with a constant step per frame, leading to different angular velocities. And each color channel has the same initial angle.

<sup>d</sup> Each channel rotates with a sinusoidal pattern with a fixed phase shift between channels. And each color channel has the same initial angle.

<sup>e</sup> Each channel rotates with a logarithmic function, creating a non-linear change over time. And each color channel has the same initial angle.

Table 5: Assessment of Rotation Results

	temporal consistency mean	temporal consistency std	color consistency mean
Same linearity	0.9652	0.0172	0.7708
Different linearity	0.9648	0.0202	0.7701
Fixed step size	0.9625	0.0190	0.7713
Sine wave phase	0.9440	0.0236	0.7815
Logarithmic growth	0.9707	0.0206	0.7741

## Funding

- The first author was supported by the National Natural Science Foundation of China (NSFC) (No. 11901079), and China Postdoctoral Science Foundation (No. 2021M700751), and the Scientific and Technological Research Program Foundation of Jilin Province (No. JJKH20190690KJ; No. JJKH20220091KJ; No. JJKH20250851KJ).
- The fourth author is supported by the Ministry of Science, Technological Development and Innovations, Republic of Serbia (No. 451-03-137/2025-03/200124).

## Conflict of Interest

The authors declare that they have no potential conflict of interest.

## Data Availability

Data sharing is not applicable to this article, as no datasets were generated or analyzed during the current study.

## References

- [1] A. Bunse-Gerstner, R. Byers, V. Mehrmann, A quaternion QR algorithm, *Numerische Mathematik*, 55 (1) (1989) 83–95.
- [2] J. Carroll, J. Chang, Analysis of individual differences in multidimensional scaling via an n-way generalization of “Eckart–Young” decomposition, *Psychometrika*, 35 (3) (1970) 283–319.
- [3] J. Chen, Q. Wang, Randomized algorithm for constrained quaternion singular value decomposition and its applications, *J. Sci. Comput.*, 59 (2025) 104.
- [4] J.C. Chou, Quaternion kinematic and dynamic differential equations, *IEEE Trans. Robot. Autom.*, 8 (1992) 53–64.
- [5] A. Einstein, The foundation of the general theory of relativity, In: The Collected Papers of Albert Einstein 6, A.J. Kox, M.J. Klein, and R. Schulmann, Princeton University Press, Princeton, NJ, 2007, 146–200.
- [6] R. Erfanifar, M. Hajarian, K. Sayevand, On Polar Decomposition of Tensors with Einstein Product and a Novel Iterative Parametric Method, *Numer. Math. Theor. Meth. Appl.*, 17 (2024) 69–92.
- [7] M. Ezoji, K. Faez, Use of matrix polar decomposition for illumination-tolerant face recognition in discrete cosine transform domain, *IET Image Process.*, 5 (2011) 25–35.
- [8] G. Golub, C. Loan, *Matrix Computations*, Johns Hopkins University Press, Baltimore, 1996.
- [9] Z. He, M. Deng, J. Pan, M.K. Ng, Diagonalization of two quaternion tensors with applications, *Appl. Math. Model.*, 148 (2025) 116278.

- [10] R.A. Horn, C.R. Johnson, *Matrix analysis*, Cambridge University Press, 2012.
- [11] M.E. Kilmer, K. Braman, N. Hao, R.C. Hoover, Third-order tensors as operators on matrices: a theoretical and computational framework with applications in imaging, *SIAM J. Matrix Anal. Appl.* 34 (1) (2013) 148–172.
- [12] M.E. Kilmer, C.D. Martin, Factorization strategies for third-order tensors, *Linear Algebra Appl.*, 435 (2011) 641–658.
- [13] T.G. Kolda, B.W. Bader, Tensor decompositions and applications, *SIAM Rev.* 51 (3) (2009) 455–500.
- [14] K. Kunze, H. Schaeben, The Bingham distribution of quaternions and its spherical Radon transform in texture analysis, *Math. Geol.*, 36 (2004) 917–943.
- [15] L.D. Lathauwer, B.D. Moor, J. Vandewalle, A multilinear singular value decomposition, *SIAM J. Matrix Anal. Appl.*, 21 (4) (2000) 1253–1278.
- [16] Y. Li, M. Wei, F. Zhang, J. Zhao, A real structure-preserving method for the quaternion LU decomposition, revisited, *Calcolo*, 54 (2017) 1553–1563.
- [17] Y. Liu, L. Chen, C. Zhu, Improved robust tensor principal component analysis via low-rank core matrix, *IEEE J. Sel. Top. Signal Process.*, 12 (6) (2018) 1378–1389.
- [18] Y. Liu, F. Wu, J. Miao, C. Li, A subspace-orbit randomized algorithm for quaternion tensor singular value decomposition based on Qt-product, *Appl. Math. Comput.*, 512 (2026) 129780.
- [19] C.D. Martin, R. Shafer, B. Larue, An order-p tensor factorization with applications in imaging, *SIAM J. Sci. Comput.*, 35 (1) (2013) A474–A490.
- [20] S. Miron, J. Flamant, N. Le Bihan, P. Chainais, D. Brie, Quaternions in signal and image processing: A comprehensive and objective overview, *IEEE Signal Process. Mag.*, 40 (2023) 26–40.
- [21] J. Pan, M.K. Ng, Block-diagonalization of quaternion circulant matrices with applications, *SIAM J. Matrix Anal. Appl.*, 45(3) (2024) 1429–1454.
- [22] Z. Qin, Z. Ming, L. Zhang, Singular value decomposition of third order quaternion tensors, *Applied Mathematics Letters*, 123 (2022) 107597.
- [23] J. Sun, X. Liu, Y. Zhang, Quaternion Tensor Completion via QR Decomposition and Nuclear Norm Minimization, *Numer. Linear Algebra Appl.*, 32 (2025) e2608.
- [24] K. Shoemake, Animating rotation with quaternion curves, in *Proceedings of the 12th Annual Conference on Computer Graphics and Interactive Techniques*, (1985) 245–254.
- [25] K. Shoemake, T. Duff, Matrix animation and polar decomposition. In *Proceedings of Graphics Interface*, (1992) 258–264.
- [26] D.A. Tarzanagh, G. Michailidis, Fast randomized algorithms for t-product based tensor operations and decompositions with applications to imaging data, *SIAM J. Imaging Sci.*, 11 (4) (2018) 2629–2664.

- [27] L. Tucker, Some mathematical notes on three-mode factor analysis, *Psychometrika*, 31 (3) (1966) 279–311.
- [28] M. Wang, W. Ma, A structure-preserving method for the quaternion LU decomposition in quaternionic quantum theory, *Comput. Phys. Commun.*, 184 (2013) 2182–2186.
- [29] M. Wang, W. Ma, A structure-preserving algorithm for the quaternion Cholesky decomposition, *Appl. Math. Comput.*, 223 (2013) 354–361.
- [30] Y. Wei, W. Ding, Theory and computation of tensors: Multi-Dimensional Arrays, Elsevier/Academic Press, London (2016).
- [31] M. Wei, Y. Li, F. Zhang, J. Zhao, Quaternion Matrix Computations, Nova Science Publisher, New York, 2018.
- [32] F. Zhang, Quaternions and matrices of quaternions, *Linear Algebra Appl.*, 251 (1997) 21–57.
- [33] F. Zhang, Y. Wei, Jordan canonical form of a partitioned complex matrix and its application to real quaternion matrices, *Communications in Algebra*, 29 (6) (2001) 2363–2375.
- [34] M. Zheng, G. Ni, Block diagonalization of block circulant quaternion matrices and the fast calculation for t-product of quaternion tensors, *Journal of Scientific Computing*, 100 (2024) 69.
- [35] Q. Zhou, S. Shen, S. Yu, D. Duan, Y. Yuan, H. Lv, H. Lin, A novel robust image watermarking algorithm based on polar decomposition and image geometric correction, *Vis. Comput.*, 40 (2024) 3303–3330.